

# Metal–Organic Frameworks and Their Composites: Synthesis and Electrochemical Applications

Fei-Yan Yi, Rui Zhang, Hailong Wang, Li-Feng Chen, Lei Han, Hai-Long Jiang,\* and Qiang Xu\*

As a youthful family of crystalline porous materials, metal–organic frameworks (MOFs), assembled by inorganic vertices (metal ions or clusters) and organic ligands, feature ultrahigh porosity, high surface area, and synthetic and structural tailorability, along with relatively easy synthesis, making them excellent candidates for a large number of applications. Recently, increasing research interest in the electrochemical fields with regard to the environment and energy has been received. Lots of MOFs have been designed, prepared, and used in electrochemical applications, exhibiting fascinating performances. Here, the rational fabrication of electrochemical-application-directed functional MOFs and MOF composites is appraised. The synthetic strategies for the enhancement of corresponding MOF electrochemical behaviors are summarized and the relationship between structure and electrochemical performance is discussed. It is expected that the summary will be helpful for the future development of related MOFs and MOF composites with an excellent electrochemical performance.

metal–oxo units) coordinating with electron-donating organic ligands. These hybrid materials have received broad concern because MOFs can be rationally synthesized with high porosities, large internal surface areas, uniform but adjustable pore sizes and structures. MOFs exhibit a tremendous growth, in terms of numerous structures, fascinating topological nets, and various application including gas storage and separation,<sup>[9–21]</sup> catalysis,<sup>[22–37]</sup> sensor,<sup>[38–41]</sup> drug delivery,<sup>[42,43]</sup> luminescence,<sup>[44,45]</sup> and others.<sup>[46–60]</sup> Apart from these applications, in recent years, there is an increasing interest in discovering the electrochemical applications in the field of supercapacitors, batteries and fuel cells, hydrogen evolution reaction (HER), oxygen evolution reaction (OER), and oxygen reduction reaction (ORR),

electrochemical decomposition of highly oxidizing and toxic compounds, electrochemical sensors, etc.

In view of the ever-growing energy demand as well as the increasing serious environmental crisis caused by the combustion of traditional fossil fuels, the pursuit of renewable energy sources resorting to the sunshine and wind, along with storage technologies, has always been a hot research subject. The intermittent feature of solar and wind sources limits their applied range, thus the effective energy storage technology is becoming a tremendous need to put electronic equipment into operation and provide electrical transportation power for commuters. Energy storage resorting to electrochemistry is thought to be one of the most promising candidates for energy storage. MOFs possess their particular advantages, in comparison with other types of porous materials including active carbon, zeolites. By selecting different metal ions and organic bridging linkers, MOFs constructed can meet the requirements of particular application through the predesign and postsynthesis methods. Various MOFs and MOF composites have been successfully used in the electrochemical areas. Moreover, MOFs as the sacrificial materials have been converted to various nanostructures, such as porous carbon, metal nanoparticles, metal oxides, and their composites with different treatments. These nanostructures with the maximum exposure of active sites inherit high surface area of MOF precursors to some extent and exhibit good performance as electrodes. For MOF-derived nanoporous functional materials, a number of reviews<sup>[61–67]</sup> and reports<sup>[68–81]</sup> have been published, which provided

## 1. Introduction


Metal–organic frameworks (MOFs) or porous coordination polymers, as a type of crystalline porous hybrid materials,<sup>[1–8]</sup> are constructed by inorganic building units (metal ions or

Dr. F.-Y. Yi, Prof. L. Han  
The School of Materials Science and Chemical Engineering  
Ningbo University  
Ningbo, Zhejiang 315211, P. R. China

R. Zhang, Prof. H.-L. Jiang  
Hefei National Laboratory for Physical Sciences at the Microscale  
Collaborative Innovation Center of Suzhou Nano Science and  
Technology  
Department of Chemistry  
University of Science and Technology of China  
Hefei, Anhui 230026, P. R. China  
E-mail: jianglab@ustc.edu.cn

Dr. H. Wang, Dr. L.-F. Chen, Prof. Q. Xu  
Research Institute of Electrochemical Energy  
National Institute of Advanced Industrial Science and Technology (AIST)  
Ikeda, Osaka 563-8577, Japan  
E-mail: q.xu@aist.go.jp

Prof. Q. Xu  
AIST—Kyoto University Chemical Energy Materials Open Innovation  
Laboratory (ChEM-OIL)  
Yoshida, Sakyo-ku, Kyoto 606-8501, Japan

 The ORCID identification number(s) for the author(s) of this article can be found under <https://doi.org/10.1002/smt.201700187>.

DOI: 10.1002/smt.201700187

comprehensive descriptions from the synthesis to applications including gas storage, clean energy, electrocatalyst, electrode, and so on. The topic here is the pristine MOFs and MOF composites directly used in the electrochemical applications, along with the synthetic methods and the relationship between structure and electrochemical performances.

It was generally considered that MOF materials were not suitable for the electrochemical application as electrodes or electrocatalysts due to their poor electron-conductive properties. Nevertheless, plenty of successful MOFs and MOF composites have been utilized in the manufacture of the electrode materials for rechargeable batteries and electrochemical sensors. In addition, they are able to promote some electrochemical reactions including HER, OER, and ORR. Therefore, it is extremely important for the rational design and synthesis strategies of MOF and MOF composites with desired electrochemical behaviors. In principle, MOFs are able to be designed and fabricated at the molecular level because of their tunable chemical compositions. Although it is still difficult for the accurate prediction and control of the overall topological structures,<sup>[82,83]</sup> the redox-active metal centers, ligands, along with the building blocks featuring electron-donating and electron-accepting ability, can be rationally introduced into MOFs, thus endow MOFs with electrochemical applications.<sup>[84–135]</sup> The functional surface area and high porosities of MOFs play crucial role in many functional properties including proton conduction, supercapacitors, and Li-based batteries. Furthermore, the development of MOF composites by introducing new electrochemical materials into pristine MOFs<sup>[136–213]</sup> enhances the MOF conductivity and boosts the electrochemical applications of MOFs. The implantation of functional materials into the MOF pores further broadens the applications of MOFs and improves the cycling performance. It is foreseeable that much more MOFs and MOF composites were used as electrode materials and electrochemical catalysts as well as some auxiliary sections in the practical electrochemical applications and exhibiting excellent performance in the future.

Here, we present a cross summary of the rational design and syntheses of MOF and MOF composites for the electrochemical applications, providing a basis for the future research. In addition, we provide an outlook for the development of MOF-derived high-performance electrochemical materials in the near future.

## 2. MOFs and MOF Composites for Electrochemical Applications

The unique ordered porous structure, high surface areas, abundant transition metals, and dispersed functional linkers of MOFs enable them to have many advantages in electrocatalysis applications. Compared with nonporous nanoparticles (NPs) or microparticles, in which only metal atoms on the surface can come into contact with the electrolyte to participate the electrochemical reactions, the metal-ion utilization of 100% in theory should be achieved in electrochemically active MOFs, if the framework exhibits adequate electron and ionic conductivities. Besides, the use of MOFs with redox-active metals or linkers as the electrode materials of Li-ion batteries (LIBs) is



**Fei-Yan Yi** received her Ph.D. in inorganic chemistry from Fujian Institute of Research on the Structure of Matter, Chinese Academy of Sciences in 2010 under the supervision of Prof. Jiang-Gao Mao. She then worked at State Key Laboratory of Rare Earth Resource Utilization, Changchun Institute of Applied Chemistry, Chinese Academy of Sciences as a postdoctoral fellow and assistant professor until 2015. She is now an associate professor in the School of Materials Science and Chemical Engineering at Ningbo University. Her research interests focus on the synthesis and application of MOFs and MOF-based functional composites.



**Hai-Long Jiang** is a professor of chemistry at University of Science and Technology of China (USTC) and Principle Investigator (PI) of Hefei National Laboratory for Physical Sciences at the Microscale. He received his Ph.D. (2008) from Fujian Institute of Research on the Structure of Matter, Chinese Academy of Sciences (CAS), and then worked with Prof. Qiang Xu at AIST (Japan) as a postdoc and JSPS fellow from 2008 to 2011. After a postdoctoral stint at Texas A&M University (USA) with Prof. Hong-Cai JOE Zhou, he joined the faculty of USTC in 2013. His main research interest is in the development of porous and nanostructured materials, crossing coordination chemistry and nanoscience, for energy-related catalysis.



**Qiang Xu** received his Ph.D. in 1994 from Osaka University. He is the Director of AIST-Kyoto University Chemical Energy Materials Open Innovation Laboratory (ChEM-OIL), Prime Senior Researcher of National Institute of Advanced Industrial Science and Technology (AIST, Japan), Adjunct Professor at Kobe University, and at Kyoto University, and a Distinguished Honorary Professor at The Hong Kong Polytechnic University. His research interests include the chemistry of nanostructured materials and their applications, especially for energy.

proposed via a slow insertion mechanism to accomplish the charge/discharge. High surface area of MOF accommodates an appropriate space for the electrochemical reaction and the ion storage during energy conversion process. However, the low conductivity and weak stability in the electrolyte cause a limitation of electrochemical applications. Therefore, the design of MOF-based materials with the target electrochemical activity and the high electron conductivity will be an important subject. With this direction, MOF composites are fabricated by hybridizing MOFs and the electrochemically active phases including sulfur, carbon-based materials (such as carbon fiber, carbon quantum dots, carbon nanotubes (CNTs), fullerene, graphite, or graphene oxide (GO)), metal nanoparticles, metal oxides, layered double hydroxides (LDHs), polymers (poly(ethylene oxide) (PEO), and composite polymer electrolyte (CPE)), as well as conductive plates. The construction of MOF composites not only effectively improves poor conductivity of pristine MOFs, but also mitigates the deficiency of each component, resulting in synergistic effects as well as novel functions. Pristine MOFs can be assembled into MOF composites with high electron conduction at a macroscopic level; however, their size-exclusion effects still limit the local charge transport due to the pore apertures. In addition, various approaches, including surface-initiated solvothermal growth, substrate corrosion, layer-by-layer assembly, and reactive electrodeposition, microwave-induced thermal deposition, as well as dip coating from colloidal solutions, have been adopted to deposit MOF on the desired substrate such as glass and glassy carbon, conductive metal plates, fluorine-doped tin oxide, indium tin oxide (ITO), and glass. Because those MOFs were directly deposited on signal transduction surfaces, the overpotential can be diminished and the efficient charge transfer can be further enhanced.

## 2.1. Pristine MOFs for Electrochemical Applications

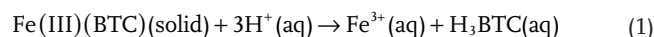
Pristine MOFs are anticipated to be directly utilized as electrolytes or electrocatalysts owing to the simple synthetic processes. For this purpose, many efforts have been paid in this field.<sup>[84–135]</sup> Pristine MOFs, which contain the electrochemical activated sites including the metal nodes and organic spacers, are able to be used in the redox-involved electrochemical

applications. In addition, the cations, ions, and protons located in/on pores and surfaces of MOFs enable this kind of materials to be a new generation of the conduction media. Nano-MOFs improve the surface/interface contact and electrolyte diffusion, electron/ion/proton conduction, thus exhibiting the enhanced electrochemical behaviors.

### 2.1.1. MOFs with Redox-Active Metal Centers

Transition metals with variable valence, including Fe, Ni, Mn, Cr, Cu, and Co, are good precursors to construct electrochemically active MOFs. These transition-metal-based MOFs will be promising candidates to replace the noble catalysts to promote some electrochemical reactions. The presence of the unsaturated metals (so-called open-metal sites) in MOFs as Lewis's acid groups can further improve such electrochemical activity for some catalytic processes.

A commercially available Basolite 300 (Fe(BTC)) MOF (BTC: benzene-1,3,5-tricarboxylate) was immobilized onto platinum and soaked in 0.5 M HCl, realizing water splitting as an efficient electrocatalyst via Fe(III/II) redox process.<sup>[84]</sup> It exhibits good cycle ability. The influence of scan rate on the peak currents was investigated during oxidation and reduction processes. Unusual "steady-state" behavior was observed, in which the peak current kept constant over a range of scan rates from 0.01 to 0.15 V s<sup>-1</sup>. A reductive dissolution can be used for explaining the mechanism of the Fe(BTC) reduction, as shown in Equation (1) and (2):



As a kind of material used for LIB electrode, MIL-101(Fe), was first reported based on the mechanism of Fe<sup>3+</sup>/Fe<sup>2+</sup> redox (Figure 1).<sup>[85]</sup> It is worthy to note that the incompletely reversible redox process (Fe<sup>3+</sup>/Fe<sup>2+</sup>) over many cycles was revealed from ex situ extended X-ray absorption fine structure spectra. As shown in Figure 1c, five reduction peaks (2.99, 2.59, 2.42, 2.27, and 2.13 V), along with two oxidation peaks (2.87 and 3.00 V),

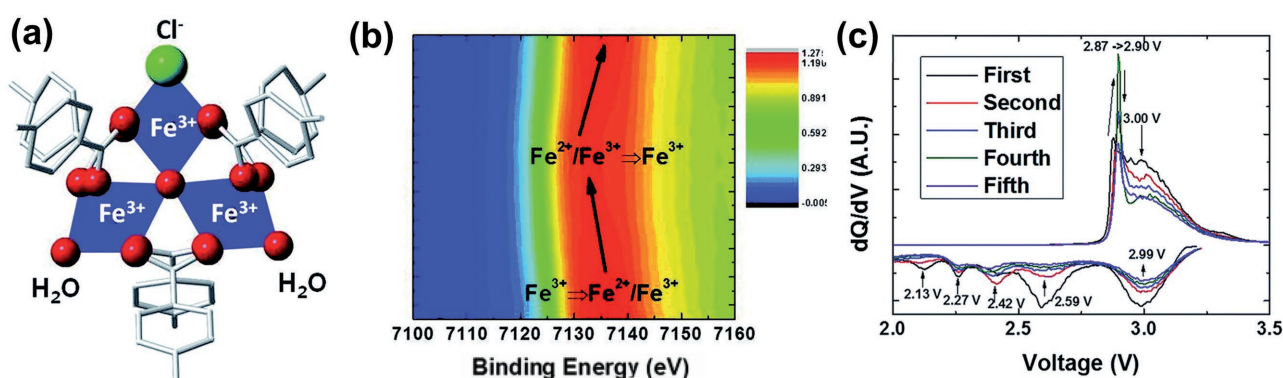


**Figure 1.** a) The secondary building unit in the structure of MIL-101(Fe). b) A reversible change of the Fe oxidation state from the contour plot of the in operando XAS XANES region vs time. c) Differential capacity ( $dQ/dV$ ) of the first five cycles at a rate of C/40. Reproduced with permission.<sup>[85]</sup> Copyright 2015, Royal Society of Chemistry.

can be observed in the first cycle. During the continuous cycles, the intensities of the redox peaks gradually become smaller. Such multiple redox peaks are attributed to different Li insertion sites in the structure of MIL-101(Fe); however, the detailed relations between redox peak and particular Li site are still not clear thus far. Furthermore, electronic structure calculations favor the hypothesis that the relaxation of Fe<sup>3+</sup> to Fe<sup>2+</sup> leads to irreversible accumulation of Li<sup>+</sup> ions for MIL-101(Fe) during the electrochemical test. With the accumulation of Li<sup>+</sup> ions, the potential Li<sup>+</sup> ion insertion sites are gradually lost in MIL-101(Fe), which causes the rapid decrease of the capacity in MIL-101(Fe). A layered coordination polymer ([Mn(tfbdc)(4,4'-bpy)(H<sub>2</sub>O)<sub>2</sub>]<sup>[86]</sup> Mn-LCP) was synthesized by Liu et al. based on the coordination between 4,4'-bipyridine (4,4'-bpy), 2,3,5,6-tetrafluoroterephthalic acid (H<sub>2</sub>tfbdc) and manganese(II) acetate tetrahydrate. The cyclic voltammetry (CV) and a galvanostatic charge/discharge cycling test were utilized for testing the electrochemical performance of Mn-LCP for lithium storage. In the CV tests, the cathodic peaks observed at around 0.1 and 0.7 V during the discharging process, and a broad anodic peak falling in the range of 0.75–1.4 V during the charging process, can be attributed to the reduction and oxidation peaks of the Mn(II)/Mn pair.

When the Mn-LCP compound was used as an anode material of Li-ion battery, an irreversible high capacity can be found in the first discharge process, and lithium storage was reversible with a capacity of up to about 390 mA h g<sup>-1</sup>. The cycling stability of the electrode can be also well demonstrated by essentially constant capacity of about 390 mA h g<sup>-1</sup> after 50 cycles. Magnetic measurements demonstrated the changes of the valence of manganese ion during charging and discharging. Such redox activities of transition-metal ions may be improved by mixed coordination of organic oxalate and inorganic phosphate, which has been described in the literature.<sup>[87]</sup> K<sub>2.5</sub>[(VO)<sub>2</sub>(HPO<sub>4</sub>)<sub>1.5</sub>(PO<sub>4</sub>)<sub>0.5</sub>(C<sub>2</sub>O<sub>4</sub>)] as a kind of metal–organic–phosphate open frameworks (MOPOFs) was synthesized by Nagarathinam et al. with redox-active vanadium as well as potential 2D transfer channels for metal ions.<sup>[87]</sup> The structural characteristic is very favorable to replace K<sup>+</sup> with Li<sup>+</sup> ions, which has been verified by the first charge–discharge cycle. Furthermore, the presence of Li<sup>+</sup> ion after several cycles can enhance the migration of Li<sup>+</sup> ions due to smaller ionic radius. In addition, CV curves of the MOPOF show its anodic and cathodic peak voltages at 4.18 V for Li extraction and 3.83 V for Li insertion, respectively. These peaks are in agreement with charge–discharge curves, corresponding to the V<sup>4+</sup>/V<sup>5+</sup> redox couple, which can be verified by X-ray absorption spectroscopy (XAS) techniques. In addition, galvanostatic cycling, ex situ Fourier transform infrared spectroscopy, and powder X-ray diffraction (PXRD) experiments were also performed to further determine the composition of electrode under charge and discharge states. Meanwhile, MOPOF systems with facile migration proton pathways represent another electrochemical application in the proton conduction.<sup>[88]</sup>

The Cu<sup>II</sup>/Cu<sup>I</sup> or Cu<sup>I</sup>/Cu couples are two redox processes that render Cu-MOFs as a potential electrocatalyst for ORR. Mao et al. revealed the electrocatalytic activity of HKUST-1 toward the ORR.<sup>[89]</sup> Cyclic voltammetry revealed that HKUST-1 was redox active, in which a pair of well-defined redox wave can be

found at ca. –0.10 V because of the redox process of Cu<sup>II</sup>/Cu<sup>I</sup> in this MOF. Besides, the reduction peak current was significantly increased, and the oxidation peak current was decreased in the presence of O<sub>2</sub> in the buffer. This phenomenon, together with a relative positive shift of O<sub>2</sub> reduction potential of the HKUST-1-modified glassy carbon (GC) electrode (GCE) in comparison with that of bare electrode, proves ORR electrocatalytic activity of HKUST-1. On account of the structural instability of HKUST-1 in aqueous media, another water-stable Cu-MOF (Cu-bipy-BTC) was synthesized. For Cu-bipy-BTC-decorated electrode and the redox wave observed at about –0.15 V in 0.1 M phosphate buffer can be assigned to the redox process of Cu<sup>II/I</sup>. After bubbling of O<sub>2</sub> into the buffer, the intensity of the reduction peak at –0.20 V was increased, while the oxidation peak was decreased, demonstrating the occurrence of ORR electrocatalytic reaction in the presence of MOF. Furthermore, an almost 4e<sup>-</sup> (3.8) reduction of O<sub>2</sub> was obtained in rotating ring-disk electrode tests, suggesting the development of a new nonplatinum electrocatalyst for ORR.<sup>[89]</sup>

Another Cu-MOF, [Cu(adp)(BIB)(H<sub>2</sub>O)]<sub>n</sub>, was prepared by the hydrothermal method by Xu and co-workers based on the rigid ligand BIB (BIB: 1,4-bisimidazolebenzene) and flexible ligand H<sub>2</sub>adp (H<sub>2</sub>adp: adipic acid).<sup>[90]</sup> The oxidation of H<sub>2</sub>O<sub>2</sub> from 0.1 × 10<sup>-6</sup> to 2.75 × 10<sup>-6</sup> M with excellent electrocatalytic activity was successfully achieved by a single-electron redox process of Cu<sup>III</sup>/Cu<sup>I</sup> pair with peaks at about 0.43 V in the solution of NaOH (0.1 M). A 2D Cu framework ((HOC<sub>2</sub>H<sub>4</sub>)<sub>2</sub>dtoaCu) composed of dimeric Cu units was prepared from the ligand of *N,N'*-bis(2-hydroxyethyl)dithioamide (HOC<sub>2</sub>H<sub>4</sub>)<sub>2</sub>dtoa (Figure 2a,b).<sup>[91]</sup> This material displayed an excellent conductivity of 3.3 × 10<sup>-4</sup> S cm<sup>-1</sup> and an excellent electrochemical behavior toward the ethanol electro-oxidation reactions (EERs). This is the first example in which non-noble-metal MOF material exhibited electrocatalysis toward EER. Experimental results demonstrated that active species of Cu with free binding sites in this MOF played a key role in such an EER electrocatalytic reaction. The peak originating from the Cu<sup>II</sup>/Cu<sup>I</sup> oxidation couple was clearly presented in the voltammogram curve (Figure 2c) and another peak at 0.71 V probably originated from the Cu<sup>I</sup>/Cu<sup>III</sup> oxidation couple.<sup>[214]</sup> The irreversible behavior might be caused due to a structural rearrangement.<sup>[215]</sup> Meanwhile, to obtain furthermore insight into the mechanism of EER, density functional theory (DFT) calculations were performed and confirmed Cu<sup>I</sup>/Cu<sup>II</sup> oxidation process.

Lu et al. synthesized a metal azolate framework, [Co<sub>2</sub>(μ-Cl)<sub>2</sub>(bbta)] (MAF-X27-Cl, H<sub>2</sub>bbta: 1*H*,5*H*-benzo(1,2-*d*:4,5-*d'*)bistriazole) (Figure 3).<sup>[92]</sup> The MAF-X27-Cl displayed high chemical stability in 0.001 M HCl and 1.0 M KOH for at least 1 week. The more interesting one is that the Cl<sup>-</sup> ligands in MAF-X27-Cl can be replaced by OH<sup>-</sup>, obtaining [Co<sub>2</sub>(μ-OH)<sub>2</sub>(bbta)] (MAF-X27-OH), which can be demonstrated by X-ray photoelectron spectroscopy (XPS) with disappearing Cl and increasing O contents, Raman spectroscopy of MAF-X27-OH with replacing Co–Cl by Co–O at 195 and 92 cm<sup>-1</sup>. The OER activity is remarkably improved due to open metal sites and hydroxide ligands of the new MAF-X27-OH material, with an overpotential of 489 mV at 2.0 mA cm<sup>-2</sup>, comparing with MAF-X27-Cl with poor OER activity (overpotential of 570 mV at 0.028 mA cm<sup>-2</sup>), although the electrical



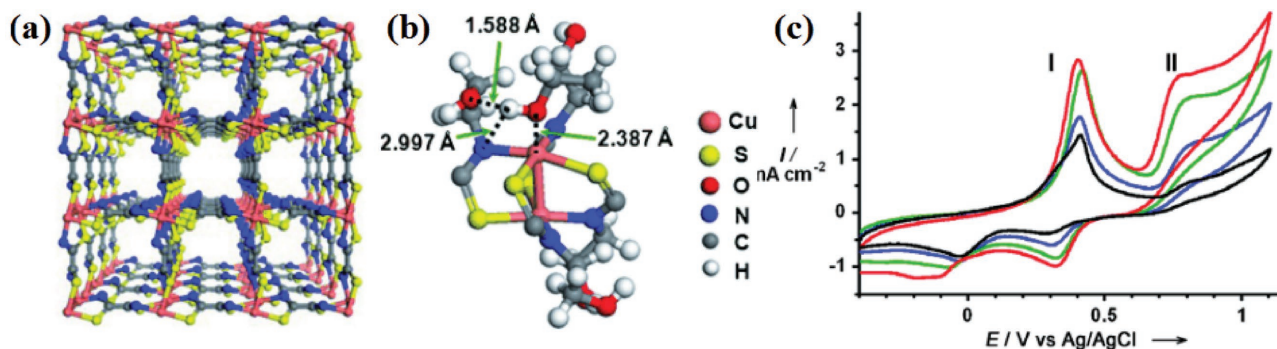


**Figure 2.** a) The crystal structure of  $[(\text{HOC}_2\text{H}_4)_2\text{dtoaCu}]$ . b) The interaction structure for  $[(\text{HOC}_2\text{H}_4)_2\text{dtoaCu}]$  and ethanol obtained from DFT calculations based on the periodic structure. c) CV curves of a glassy carbon electrode coated with  $[(\text{HOC}_2\text{H}_4)_2\text{dtoaCu}]$  in 0.5 M  $\text{H}_2\text{SO}_4$  with different concentrations of ethanol (black 0.0 M, blue 0.5 M, green 1.0 M, red 2.0 M ethanol). Sweep rate =  $100 \text{ mV s}^{-1}$ . Reproduced with permission.<sup>[91]</sup> Copyright 2010, Wiley-VCH.

conductivity MAF-X27-Cl ( $2.2 \times 10^{-7} \text{ S cm}^{-1}$ ) is much higher than the one of MAF-X27-OH with  $2.2 \times 10^{-9} \text{ S cm}^{-1}$ . The result ascribes the increasing electrocatalytic activity by  $\mu\text{-OH}^-$  ligands mainly to the change of chemical reaction pathway over electrical conductivity. Furthermore, isotope tracing experiments demonstrate that the OER mechanism of MAF-X27-OH is put down to direct participation of the  $\mu\text{-OH}^-$  ligands or the intra-framework coupling pathway in the OER process. When MAF-X27-OH was grown directly on Cu foil, its OER electrocatalytic activity was greatly improved with overpotentials as low as 292 mV at  $10 \text{ mA cm}^{-2}$ , which is the best value among catalysts reported. Thus, this MOF material is a very good OER catalyst with high electrocatalysis performance and stability/durability, and opens up new possibilities for OER catalysts.

### 2.1.2. MOFs with Mixed Metal Centers

Different metal centers will lead to the different electrochemical behaviors of MOFs based on respective electron configurations; therefore, an MOF with mixed metal centers might be a good strategy to discover new electrochemical behaviors.

A new MOF with mixed metal ion (Fe/Co) was synthesized by Yin and co-workers using trimesic acid as organic linker.<sup>[93]</sup> This material exhibits an excellent bifunctional catalytic activity for OER and ORR in alkaline solution. Rotating disk electrode tests indicate that at relatively positive potentials, the two-electron transfer predominates; however, at more negative potentials, the four-electron transfer gradually comes into prominence. This work demonstrates that the mixed-metal method for constructing MOF with bifunctional catalytic activity is effective instead of precious metal catalyst.

A novel MOF  $\{[\text{Fe}_3(\mu_3\text{-O})(\text{bdc})_3]_4[\text{Co}_2(\text{na})_4(\text{L}^T)_2]_3\}$  (Hna: nicotinic acid;  $\text{L}^T$ : terminal ligand) has been constructed by a two-step, single crystal to single crystal, post-synthetic strategy.<sup>[94]</sup> The formation of this hybrid MOF is attributed to that  $[\text{Fe}_3(\mu_3\text{-O})(\text{bdc})_3]_4[\text{Fe}(\text{na})_4(\text{L}^T)]_3$  can release its  $\text{Fe}(\text{na})_4(\text{L}^T)$  fragment to obtain  $[\text{Fe}_3(\mu_3\text{-O})(\text{bdc})_3]_4$  with open metal sites for binding the dicobalt cluster  $\text{Co}_2(\text{na})_4(\text{L}^T)_2$ . The paddlewheel-type clusters  $\text{Co}_2(\text{RCOO})_4(\text{L}^T)_2$  (R: a substituent group) were usually used as electrocatalytically active sites. The mixed-metal MOF is thermal-, water-, and alkaline stable, displaying an extraordinary electrocatalytic OER activity in water at pH = 13 with overpotential as low as 225 mV at  $10.0 \text{ mA cm}^{-2}$ . Moreover, an ultrathin NiCo bimetal-organic framework nanosheet (NiCo-UMOFNs)

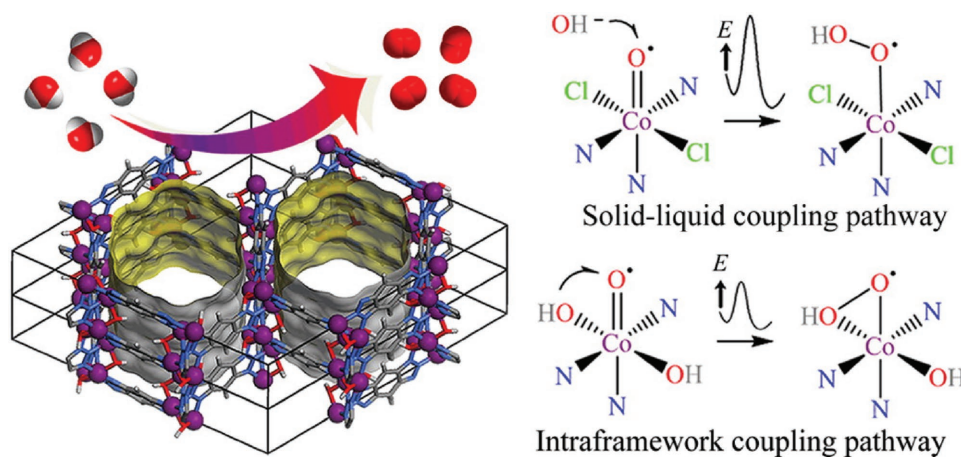


**Figure 3.** 3D coordination network and pore surface structures of MAF-X27-OH, as well as solid-liquid coupling pathway for MAF-X27-Cl, and intraframework coupling pathway for MAF-X27-OH. Reproduced with permission.<sup>[92]</sup> Copyright 2016, American Chemical Society.

as a promising electrocatalyst for OER in alkaline conditions<sup>[95]</sup> was prepared by ultrasonication at room temperature from a mixed solution of Ni<sup>2+</sup>, Co<sup>2+</sup>, and benzenedicarboxylic acid (BDC). It was loaded on copper foam, showing a low onset potential (1.39 V) and an overpotential (189 mV) at 10 mA cm<sup>-2</sup>. At a constant overpotential of 0.25 V, the current density is very stable for at least 200 h and the associated Faradaic efficiency is as high as 99.3%. In the NiCo-UMOFNs, the ultrathin nature makes them well dispersed in aqueous solution for at least several months. Those unsaturated metal centers dominate the active sites of the electrocatalytic OER. XAS data as well as DFT calculations propose the bimetal coupling mechanism of Co and Ni in the electrocatalytic OER. Moreover, the NiCo-UMOFNs catalyst exhibits a long-term catalytic stability.

Polyoxometalates (POMs), primarily soluble anionic metal oxide clusters with redox-active high-valence transition metals (W<sup>VI</sup>, Mo<sup>V,VI</sup>, and V<sup>IV,V</sup>), exhibit great potential in catalysis.<sup>[216–223]</sup> However, the significant solubility of pure POMs in reaction systems greatly impedes their applications to solid catalysts, where limited recyclability is due to the disorganization of active sites. In order to resolve the recyclability, POMs are usually fixed on porous supports with Lewis acidity. POM-based MOFs, so-called POMOFs, are a family of mixed metal MOFs,<sup>[96–99]</sup> in which POMs as metal cluster were connected to one another through organic linkers or filled in pores to form POMOFs. POMOFs feature the superiorities of POMs and MOFs and make up for individual shortcomings. Thus, this type of materials as electrocatalysts displays excellent electrochemical behaviors.

POMOFs were verified as the electrochemical catalysts in 2009. A POMOF,<sup>[96]</sup> [NBu<sub>4</sub>]<sub>3</sub>[PMo<sup>V</sup><sub>8</sub>Mo<sup>VI</sup><sub>4</sub>O<sub>36</sub>(OH)<sub>4</sub>Zn<sub>4</sub>(BDC)<sub>2</sub>·2H<sub>2</sub>O (NBu<sub>4</sub>: tetrabutylammonium), was designed and synthesized based on zinc salt, benzenedicarboxylate (BDC) ligand, and  $\epsilon$ -type Keggin POMs. This POMOF was insoluble in organic solvents and showed excellent activity toward the bromate reduction. POMOF maintained the original electrochemical activity of  $\epsilon$ -Keggin POM and exhibited an enhanced electrocatalytic performance in comparison with that of the pure POM. As bromate concentration gradually increased, the cathodic current of the second reduction wave increased and the corresponding anodic current gradually decreased. The mechanism of this reaction was described as a six-electron process.

Another 3D POMOF, (TBA)<sub>3</sub>[PMo<sup>V</sup><sub>8</sub>Mo<sup>VI</sup><sub>4</sub>O<sub>36</sub>(OH)<sub>4</sub>Zn<sub>4</sub>]-[C<sub>6</sub>H<sub>3</sub>(COO)<sub>3</sub>]<sub>4/3</sub>·36H<sub>2</sub>O ( $\epsilon$ (trim)<sub>4/3</sub>), was synthesized by Nohra et al.,<sup>[97]</sup> which is built of molecular Keggin units of tetrahedral  $\epsilon$ -Keggin POMs and triangular BTC linkers (denoted as “trim”) with its channels occupied by tetrabutylammonium (TBA) counterions. As a comparison, another two POMOFs were synthesized, namely (TBA)<sub>3</sub>[PMo<sup>V</sup><sub>8</sub>Mo<sup>VI</sup><sub>4</sub>O<sub>37</sub>(OH)<sub>3</sub>Zn<sub>4</sub>]-[C<sub>6</sub>H<sub>3</sub>(COO)<sub>3</sub>]<sub>3</sub> ( $\epsilon_2$ (trim)<sub>2</sub>) and (TBA)<sub>3</sub>[PMo<sup>V</sup><sub>8</sub>Mo<sup>VI</sup><sub>4</sub>O<sub>37</sub>(OH)<sub>3</sub>Zn<sub>4</sub>]-[C<sub>6</sub>H<sub>3</sub>(COO)<sub>3</sub>]<sub>3</sub>·8H<sub>2</sub>O ( $[\epsilon$ (trim)] <sub>$\infty$</sub> ), respectively, in which the building units of molecular Keggin were replaced by a dimerized form in  $\epsilon_2$ (trim)<sub>2</sub> and 1D zigzag chain in  $[\epsilon$ (trim)] <sub>$\infty$</sub> . They were adsorbed directly on glassy carbon or trapped in carbon paste (CPE) to form the modified electrodes for the experiment of electrocatalytic HER. The results reveal that the onset potential of POMOF-based electrode,  $\epsilon$ (trim)<sub>4/3</sub>/CPE, displays an  $\approx$ 260 mV anodic shift than that of platinum electrode,

indicating that it is much more active than platinum electrode. The turnover number is as high as  $1.2 \times 10^5$ . The POMOF/CPE electrodes are extremely stable. First, it shows no obvious change after cycles of hundreds of times. Second, the behaviors of these electrodes also do not exhibit transformation upon immersing in solution and keep stable several months in the air. This work is the first report about non-noble metal POM-based HER electrode showing a high turnover frequency of  $\approx 6.7$  s<sup>-1</sup> with an overpotential value ( $\eta = 200$  mV) in aqueous medium. Electrocatalytic mechanistic pathway for the HER is also analyzed. Cyclic voltammogram of  $\epsilon_2$ (trim)<sub>2</sub> in acidic solution (pH = 1) illustrates two clearly defined bielectronic waves for Mo reduction followed by two closely spaced waves. These continuous electron processes are due to the chemically reversible reduction of Mo<sup>VI</sup> centers. As is well known, the Mo<sup>V</sup> states in these POMOFs are also electroactive. The similar electrocatalytic behavior still exists for the reduction of the POMOFs in  $\epsilon$ (trim)<sub>4/3</sub> and  $[\epsilon$ (trim)] <sub>$\infty$</sub> .

Qin et al. synthesized two novel POMOFs, [TBA]<sub>3</sub>[ $\epsilon$ -PMo<sup>V</sup><sub>8</sub>Mo<sup>VI</sup><sub>4</sub>O<sub>36</sub>(OH)<sub>4</sub>Zn<sub>4</sub>][BTB]<sub>4/3</sub>·xGuest (NENU-500, BTB: benzene tribenzoate) and [TBA]<sub>3</sub>[ $\epsilon$ -PMo<sup>V</sup><sub>8</sub>Mo<sup>VI</sup><sub>4</sub>O<sub>37</sub>(OH)<sub>3</sub>Zn<sub>4</sub>]-[BPT] (NENU-501, BPT: [1,1'-biphenyl]-3,4',5-tricarboxylate), based on similar POM building unit and a longer triangular ligand.<sup>[98]</sup> They are 3D open frameworks, and TBA<sup>+</sup> ions reside inside the open channel to balance the anionic frameworks. They functioned as electrocatalysts exhibiting high activities for the HER. NENU-500 exhibits the higher activity with an overpotential of 180 mV and a Tafel slope of 96 mV dec<sup>-1</sup>, along with the current density of up to 10 mA cm<sup>-2</sup> at 237 mV. Both of them display excellent stability even after 2000 cycles.

The open metal sites in MOF structures have been demonstrated a helpful factor for electrochemical applications. Two octamolybdate-based MOFs, namely, Cu<sub>3</sub>(Mo<sub>8</sub>O<sub>26</sub>)(H<sub>2</sub>O)<sub>2</sub>(OH)<sub>2</sub>(L<sup>1</sup>)<sub>4</sub> (L<sup>1</sup>: 4H-4-amino-1,2,4-triazole) (1) and Ag<sub>4</sub>(Mo<sub>8</sub>O<sub>26</sub>)(L<sup>2</sup>)<sub>2.5</sub>(H<sub>2</sub>O) (L<sup>2</sup>: 3,5-dimethyl-4-amino-4H-1,2,4-triazole) (2), were prepared by Lin and co-workers, and displayed the electrochemical activity for the HER.<sup>[100]</sup> Two POMOFs contain unsaturated coordinated metal centers. Cyclic voltammograms of POMOF-modified carbon glassy electrode revealed that the two complexes demonstrated excellent HER activities, in terms of the lowered overpotentials and improved currents. The overpotential of complex 1 ( $\eta = -0.43$  V), higher than complex 2 ( $\eta = -0.49$  V), suggests that the former electrode is better than the latter one, which is associated with the structures with different unsaturated coordinated metal centers. The enhanced current for HER may be attributed to the redox property of the [Mo<sub>8</sub>O<sub>26</sub>]<sup>4-</sup> polyanion overlapped by the potential of the proton reduction.

### 2.1.3. MOFs with Functional Linkers

The introduction of functional linkers into MOF is a good strategy to improve the charge/electron transfer inside the framework. In 2013, a redox-active ligand of *N,N'*-bis-(4-pyridyl)-phthalamide) ligand (L<sup>3</sup>) was used for the fabrication of porous MOFs of Zn<sub>6</sub>(BPC)<sub>6</sub>(L<sup>3</sup>)<sub>3</sub>·9DMF (H<sub>2</sub>BPC: 4,4'-biphenyldicarboxylic acid) (3) and Cd<sub>2</sub>(TDC)<sub>2</sub>(L<sup>3</sup>)<sub>2</sub>·4H<sub>2</sub>O (H<sub>2</sub>TDC: 2,5-thiophenedicarboxylic acid) (4).<sup>[101]</sup> In an aqueous electrolyte, these

two Zn- and Cd-based MOFs offer a large voltage window of 2.6 V as supercapacitor electrode materials, as well as respective specific capacitances (SCs) much higher than that of the bare GCE. When 3-GCE is utilized, a reversible redox couple can be found with  $E_{pa} = 0.12$  V of anodic and  $E_{pc} = 0.40$  V of cathodic peak potentials versus the saturated calomel electrode (SCE), respectively. Similar reversible redox peaks can be also observed for 4-modified electrode (4-GCE) in 1 M  $\text{Li}_2\text{SO}_4$  aqueous solution. Complexes **3** and **4** show a pseudocapacitive behavior, ascribed to the redox-active  $\text{L}^3$  ligand in their structures. In addition, one group of reversible anodic peak at  $E_{pa} = -0.89$  V and cathodic peak at  $E_{pc} = -0.72$  V vs SCE for 4-GCE may arise from the thiophene functional group in the  $\text{TDC}^{2-}$  ligand. The potentials of the  $\text{H}_2$  and  $\text{O}_2$  generation at 4-GCE move to  $-1.5$  and  $1.3$  V vs SCE, respectively, suggesting that water splitting is hampered by complex **4**. A current density of  $18.75 \text{ mA g}^{-1}$  can still be observed after continuous cycling for 500 times, with no significant loss in capacitance, proving that they are stable.

Another redox-active ligand, 2,7-anthraquinonedicarboxylic acid (2,7- $\text{H}_2\text{AQDC}$ ), was used for the construction of a new microporous MOF,  $\text{Cu}_2(\text{Ac})_4$  paddlewheels.<sup>[102]</sup> As previously reported, anthraquinone (AQ) exhibit two reversible redox steps with one electron uptake; therefore, they can be employed as cathode active materials in lithium batteries. In situ X-ray absorption near edge structure (XANES) analysis and cyclic voltammetry reveal that the metal cluster nodes of  $\text{Cu}_2(\text{Ac})_4$  paddlewheels and anthraquinone groups in  $\text{Cu}_2(2,7\text{-AQDC})$  were simultaneously involved in the reduction during the discharge process for lithium batteries (Figure 4). With the voltage window and scan current of 4.0–1.7 V and 1 mA, respectively, an initial specific capacity of  $147 \text{ mA h g}^{-1}$  was acquired, and the capacity was stabilized to  $\approx 105 \text{ mA h g}^{-1}$  within 50 cycles. This MOF is the first example where both metal and ligand are redox active. Furthermore, this MOF is highly robust, and extremely high recyclability of batteries can be achieved by controlling the voltage window of operation.

A novel  $\text{Ni}_3(\text{HITP})_2$  MOF was fabricated from the ligand of 2,3,6,7,10,11-hexamino-triphenylene (HITP),<sup>[103]</sup> in which HITP connected metal centers into a 2D layer, further stacking a 3D supermolecular structure by  $\pi$ -conjugated interaction. The 1D cylindrical channels of  $\approx 1.5$  nm diameter can be observed.

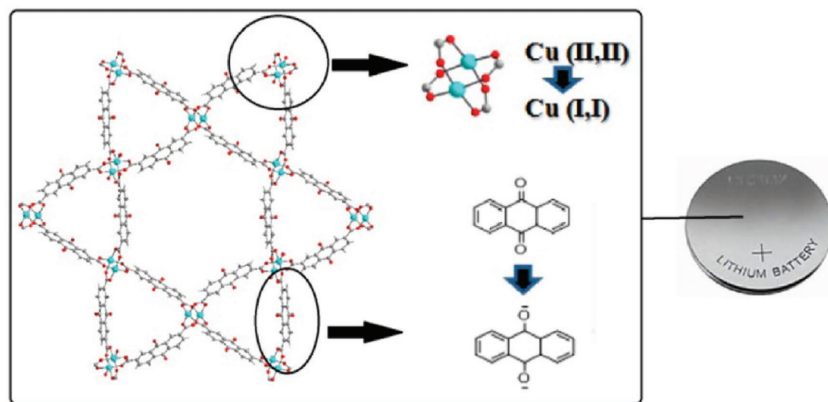


**Figure 4.** A single-layered framework as well as the production of reduction for  $\text{Cu}^{\text{II,II}}_2(\text{Ac})_4$  clusters and AQ. Reproduced with permission.<sup>[102]</sup> Copyright 2015, American Chemical Society.

$\text{Ni}_3(\text{HITP})_2$  as a conductive MOF with large open channel and high surface area can accommodate large electrolyte ions for electrochemical double layer capacitors. An MOF-based device has been prepared by using  $\text{Ni}_3(\text{HITP})_2$  as a single-component electrode without involving any conductive additives and organic binders. The CV, galvanostatic charge and discharge of a symmetrical cell show that  $\text{Ni}_3(\text{HITP})_2$  exhibits nearly rectangular and triangular traces, respectively, with a gravimetric capacitance of  $111 \text{ F g}^{-1}$  at a discharge rate of  $0.05 \text{ A g}^{-1}$ . The supercapacitor disclosed a high capacity retention between 0 and 1 V at  $2 \text{ A g}^{-1}$  over 10 000 cycles and a very high surface area normalized capacitance of  $18 \mu\text{F cm}^{-2}$ . The superior supercapacitor behavior is associated with the electrical conductivity greater than  $5000 \text{ S m}^{-1}$ .

A functional Zn-MOF,  $\text{Zn}(\text{IM})_{1.5}(\text{abIM})_{0.5}$ , was constructed by 2-aminobenzimidazole (abIM) and imidazole (IM),<sup>[104]</sup> because abIM combined the characteristics of phenyl with hydrophobic and rigid group, amine and imidazolate groups as binding sites interacting with Li atoms. In this Zn-MOF, amine and phenyl groups were located around the cavities, forming a unique pore environment. Such functional porosity makes it a promising candidate as a bifunctionalized MOFs (BMOFs) for Li-ion battery electrode. Besides, its thermal stability is much better than that of most amine-decorated MOFs with usually decomposition temperature lower than  $400 \text{ }^\circ\text{C}$ .<sup>[224,225]</sup> In addition, BMOF displays the excellent chemical stability even in aqueous and organic media, favorable for the electrochemical applications. Experiments and DFT calculations proved that its framework remained intact after the tenth cycles without further capacity loss (200 cycles) from the discharge/charge result. In the discharge processes of BMOF-based anode at 100, 200, and  $400 \text{ mA g}^{-1}$ , the specific capacity was stabilized after the tenth cycle without further capacity loss (200 cycles). In particular, an almost 100% Coulombic efficiency was maintained by the BMOF anode discharged at  $400 \text{ mA g}^{-1}$  after 200 cycles. This Li-ion battery working mechanism is different from the above redox transformation of metal centers.<sup>[84,89,90]</sup> The interaction between Li and amine groups/N atoms in IM is of great significance for the discharge and charge processes.

Another Zr-MOF (UiO-66) with high stability was successfully synthesized under stirring.<sup>[105]</sup> When different reaction temperatures were selected, MOFs with different degrees of crystallization and particle sizes can be synthesized, namely, Zr-MOF-1, Zr-MOF-2, Zr-MOF-3, and Zr-MOF-4. X-ray diffraction (XRD) patterns demonstrated that Zr-MOF-4 had better crystallinity compared with Zr-MOF-1, Zn-MOF-2, and Zr-MOF-3. Scanning electron microscopy (SEM) results revealed that the particle sizes were 100, 200, 450, and 500 nm for Zr-MOF-1, Zr-MOF-2, Zr-MOF-3, and Zr-MOF-4, respectively. Based on the nitrogen adsorption–desorption isotherms, the Brunauer–Emmett–Teller (BET) specific surface area is  $1047 \text{ m}^2 \text{ g}^{-1}$  for Zr-MOF-1,  $933 \text{ m}^2 \text{ g}^{-1}$  for Zr-MOF-2,  $732 \text{ m}^2 \text{ g}^{-1}$  for Zr-MOF-3, and  $596 \text{ m}^2 \text{ g}^{-1}$  for Zr-MOF-4, respectively. Their electrochemical application in supercapacitors was observed.



Zr-MOF-1 showed the maximum specific capacitance, reaching  $1144 \text{ F g}^{-1}$  at a scan rate of  $5 \text{ mV s}^{-1}$  and  $50 \text{ }^\circ\text{C}$ , which is much higher than Zr-MOF-2 ( $811 \text{ F g}^{-1}$ ), Zr-MOF-3 ( $517 \text{ F g}^{-1}$ ), and Zr-MOF-4 ( $207 \text{ F g}^{-1}$ ). The data of electrochemical measurements proved that the Zr-MOF-1 had outstanding capacitance performance and high cycling stability over 2000 cycles. Zr-MOF-1 will be a promising supercapacitor electrode material. In a common electrochemical capacitor, where the charges are collected within the double layers mainly by electrostatic force, its CV curve is close to an ideal rectangular shape. Nevertheless, in this work, quasi-symmetric redox peaks are apparent in the CV curves, which demonstrate that the redox mechanism, which the measured capacitance follows, differs from that of electric double layer capacitors. In other words, through the reversible electrochemical reactions, the ions should be adsorbed on the surface of the electrode. Thus, Zr-MOF-1 has a larger surface area, and the electrode can collect substantial charges to realize higher capacitances.

#### 2.1.4. MOFs with Unique Pores

Li-O<sub>2</sub> batteries have attracted wide research interest because of their high theoretical gravimetric energy density of  $3500 \text{ W h kg}^{-1}$ . Ordinarily, a Li-O<sub>2</sub> battery is made up of a metal anode (lithium), an Li<sup>+</sup> conduction electrolyte, and an O<sub>2</sub> electrode. Separate kinds of MOFs, such as MOF-5, HKUST-1, and M-MOF-74 (M = Co, Mg, and Mn), with high surface areas and unique pore environment were selected and used as O<sub>2</sub> electrodes, which facilitate lithium and oxygen transport as well as the deposition of discharge products (Figure 5).<sup>[106]</sup> The concentration of O<sub>2</sub> in the micropores of these MOFs was significantly increased at 1 atm and 273 K, which was larger than pure oxygen. The discharge capacities of Li-O<sub>2</sub> battery built from the cathode of MOFs and carbon black (Super P) exceed that of the sole Super P cathode. The electrochemical tests show that all the cells display the very stable operating voltages of 2.6–2.7 V, which are similar to many Li-O<sub>2</sub> cells manufactured. They also exhibit the very high discharge capacities for batteries,  $4170 \text{ mA h g}^{-1}$  for HKUST-1,  $4560 \text{ mA h g}^{-1}$  for Mg-MOF-74, and  $3630 \text{ mA h g}^{-1}$  for Co-MOF-74, which are much better than that of carbon black alone ( $2170 \text{ mA h g}^{-1}$ ). Significantly, Mn-MOF-74 has the highest discharge capacity of  $9420 \text{ mA h g}^{-1}$ . The high capacities of HKUST-1 and M-MOF-74 are attributed to the open metal sites of MOFs located at the pore surfaces which strongly interact with oxygen molecules and ions. Therefore, M-MOF-74 achieves the highest discharge capacity with 3.3 accessible open metal sites per  $100 \text{ \AA}^2$  on the inner surface.

High proton conductivity is vital for the properties of solid electrolyte in fuel cells. In order to realize high proton

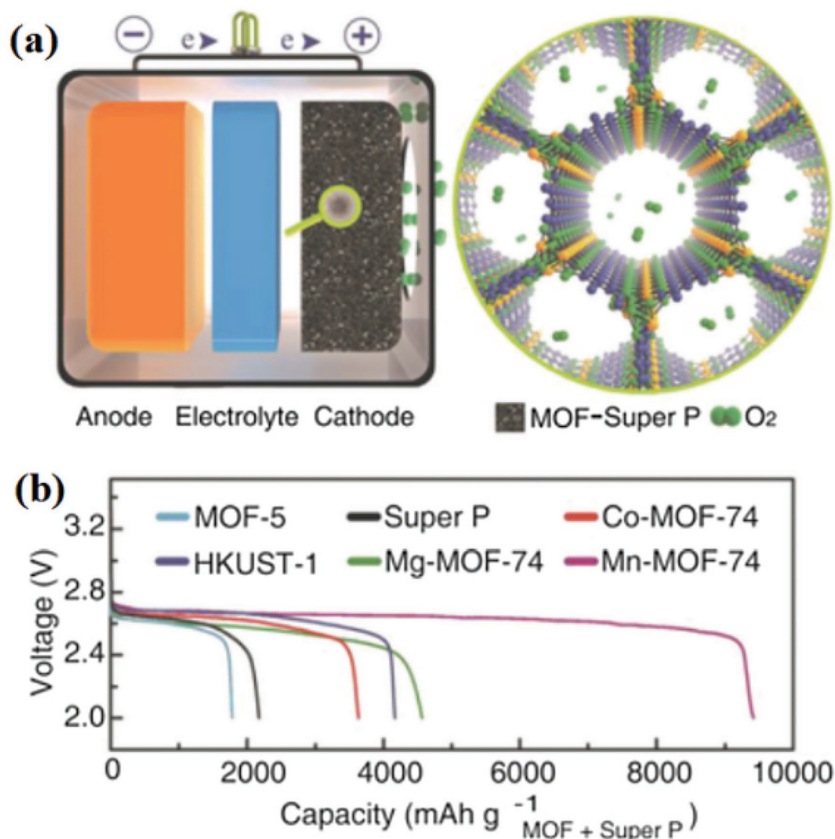


**Figure 5.** a) Schematic diagram of an Li-O<sub>2</sub> battery using MOF-Super P composite as the O<sub>2</sub> electrode. b) Discharge curve of the Li-O<sub>2</sub> cells using MOF-Super P composites or Super P with a current of  $50 \text{ mA g}^{-1}$  under O<sub>2</sub> atmosphere at room temperature. Reproduced with permission.<sup>[106]</sup> Copyright 2014, Wiley-VCH.

conductivity, hydrophobic pores are often integrated with hydrophilic ones. Recently, MOFs are thought to be a new type of proton conductors and transporters because they can accommodate highly concentrated mobile ions or provide feasible proton-transfer pathways. For the protonic conduction behaviors of MOFs, the incorporation of hydrophobic and hydrophilic pores, rich proton carriers, and fast proton-transfer pathways are important factors to influence the proton mobility and proton-transfer efficiency. The design strategies have been summarized in many reviews.<sup>[59,109]</sup> These reviews have described and discussed the design and synthesis of proton-conducting MOFs, as well as various influencing factors. In the field of proton-conducting applications for MOFs, a great deal of work has been reported with excellent performance.<sup>[88,108–126]</sup> Herein, we just discussed several examples of MOFs to highlight the applications of MOF with unique pores in the proton conduction under anhydrous conditions and high temperatures.

The implantation of proton-carrier molecules (e.g., imidazole, histamine) into the MOF channels was a successful method to develop high-temperature proton conductors.<sup>[109]</sup> It is important that comparable sizes of pore diameters and guests contribute to improving the mobility of guest molecules and ions. The MOFs reported usually display conductivity in the range



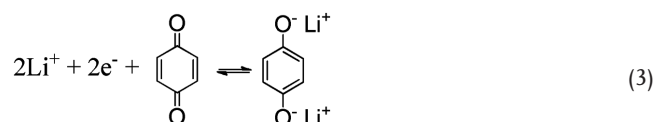
of  $10^{-3}$ – $10^{-7}$  S  $\text{cm}^{-1}$ . The MOF material with a proton-carrier molecule can generate a high proton conductivity of larger than  $10^{-3}$  S  $\text{cm}^{-1}$  at high temperature due to strong host–guest interactions. An Al(OH)(14ndc) MOF (14ndc: 1,4-naphthalenedicarboxylate) has been synthesized and it contains 1D pores with a diameter of 1 nm,<sup>[108]</sup> which accommodates imidazole molecules as guest molecules. This MOF confines the imidazole molecules in the pores to form an anisotropic alignment, which affords high mobility and yields a proton conductivity of  $2.2 \times 10^{-5}$  S  $\text{cm}^{-1}$  at 120 °C under anhydrous conditions. The suitable pore sizes and shapes to match guests are important factors in the confinement of guest rotation dynamics and the enhancement of the proton mobility. Another MOF,<sup>[125]</sup> [Na<sub>3</sub>(2,4,6-trihydroxy-1,3,5-benzenetrisulfonate)] $\times$ (1,2,4-triazole) ( $x = 0.6$ ), was synthesized by introducing 1,2,4-triazole into the MOF pores. Here, the 1,2,4-triazole is a starting material in the construction of MOFs with a proton conductivity of  $5 \times 10^{-4}$  S  $\text{cm}^{-1}$  at 150 °C. Moreover, the MOF was fabricated into a membrane, and a high voltage of 1.18 V was observed at 100 °C for the MOF-based fuel cell based on open-circuit voltage (OCV).

A sample is prepared by directly impregnating nonvolatile acids H<sub>2</sub>SO<sub>4</sub> and H<sub>3</sub>PO<sub>4</sub> into MOFs to improve the amount and mobility of proton carriers and thus to target the better proton conductors. Such a method requires highly stable MOFs in strong acidic environment. Among the few examples, chromium(III) terephthalate MIL-101 thus has been chosen as a host to encapsulate the either H<sub>2</sub>SO<sub>4</sub> or H<sub>3</sub>PO<sub>4</sub> molecules in the pores.<sup>[124]</sup> The resulting MIL-101@H<sub>2</sub>SO<sub>4</sub> and MIL-101@H<sub>3</sub>PO<sub>4</sub> hybrids display high proton conductivities in a broad temperature scope from 40 to 150 °C. Even after the release of water molecules at 150 °C, proton conductivities of  $1 \times 10^{-2}$  and  $3 \times 10^{-3}$  S  $\text{cm}^{-1}$ , respectively, are achieved at 150 °C and low relative humidity (RH) of 0.13%. Besides the impregnation of inorganic phosphate acid as a proton-hopping site to the pores of MOF, phosphate acid has been used as starting materials to react with the metal ion to form MOF with the help of secondary N-containing heterocycle ligands. For example, the room-temperature reaction between zinc oxide, 1,2,4-triazole (TzH), and phosphoric acid (H<sub>3</sub>PO<sub>4</sub>) generates a sample with the chemical composition of [Zn(H<sub>2</sub>PO<sub>4</sub>)<sub>2</sub>(TzH)<sub>2</sub>]<sub>n</sub>.<sup>[123]</sup> Zn ions were bridged by orthophosphate and protonated TzH<sup>+</sup> ion, providing a 2D layer. In the meanwhile, the neighboring layers are connected by hydrogen bond interaction between the coordinated orthophosphate ions. The conductivities are  $1.4 \times 10^{-6}$  S  $\text{cm}^{-1}$  for the bulk crystals and  $1.8 \times 10^{-7}$  S  $\text{cm}^{-1}$  for the powder at 45 °C. The overall conductivity is  $\approx 10^{-4}$  S  $\text{cm}^{-1}$  at 150 °C. A dry H<sub>2</sub>/air cell was manufactured using this sample-involved membrane–electrode assembly. OCV was measured as  $\approx 0.65$  V and 0.50 V at 25 and 130 °C, respectively. This strategy provides a low-cost and facile way to synthesize new proton conductors.

Except the fact that the formation of acid–base pairs with basic sites and strong acids (H<sub>2</sub>SO<sub>4</sub> and H<sub>3</sub>PO<sub>4</sub>) in polymer can improve the proton conduction, it is expected that efficient proton transport is still feasible under anhydrous, humidified conditions and elevated temperature. Ghosh and co-workers selectively synthesized an oxalate-based MOF {[ (Me<sub>2</sub>NH<sub>2</sub>)<sub>3</sub>(SO<sub>4</sub>)<sub>2</sub>][Zn<sub>2</sub>(ox)<sub>3</sub>]}<sub>n</sub> (ox: oxalate),<sup>[126]</sup> which consisted of a 3D anionic framework [Zn<sub>2</sub>(ox)<sub>3</sub>]<sup>2-</sup>, and an interpenetrated cationic supramolecular net [(Me<sub>2</sub>NH<sub>2</sub>)<sub>3</sub>SO<sub>4</sub>]<sup>+</sup>, in which a

sulfate ion is connected to six {Me<sub>2</sub>NH<sub>2</sub>}<sup>+</sup> cations by electrostatic interactions and hydrogen bonds of N–H...O, forming a 3D supramolecular net. Such a connected hydrogen-bonded network is significant for efficient proton conduction. PXRD patterns under variable temperature at 30–150 °C and in water overnight demonstrate the water stability of this compound. The test result displays that the compound shows a high proton conductivity of  $1 \times 10^{-4}$  S  $\text{cm}^{-1}$  under anhydrous condition at 150 °C, which is better than other proton-conducting MOFs. Under 98% RH, it also exhibits a water-assisted proton conductivity of  $4.2 \times 10^{-2}$  S  $\text{cm}^{-1}$ . This is the highest value for other proton-conducting materials based on MOF frameworks reported up to now. Under anhydrous condition, the high proton transfer is due to the concentration of the carrier and the efficiency of the proton conduction. In this compound, these characteristics contribute to fast and efficient transfer of protons, such as ordered arrangement of 3D proton carriers and connected 3D hydrogen bonding of [(Me<sub>2</sub>NH<sub>2</sub>)<sub>3</sub>SO<sub>4</sub>]<sup>+</sup>. Under humidified conditions, the mechanism of proton conduction should be ascribed to acid–base pair units, which is similar to that reported in other reports in the literature.<sup>[109]</sup>

MOFs with the high porosities and surface areas have also been demonstrated as good candidates for the LIB application. Combarieu et al. used MIL-53(Fe) [(Fe<sup>III</sup> (OH, F)bdc] as the host to synthesize a hybrid material,<sup>[135]</sup> namely MIL-53(Fe)<sub>y</sub>–(quinone)<sub>y</sub> ( $y = 1$ ) by introducing the electroactive guest 1,4-benzoquinone molecule with a molar ratio of 1:1, and the structure of MIL-53(Fe)<sub>y</sub>–quinone has been verified by <sup>13</sup>C NMR spectra and synchrotron X-ray powder diffraction. Two redox species can be found in the new MIL-53(Fe)<sub>y</sub>–quinone phase: the Fe<sup>3+</sup>/Fe<sup>2+</sup> redox couple and the quinone molecules, which are electrochemically active toward Li, as exhibited in the following reaction (3):



Electrochemical tests confirm that the quinone-free phase (MIL-53(Fe)) can reversibly adsorb 0.6 Li<sup>+</sup> per formula unit and the gravimetric capacity reaches 93 mA h g<sup>-1</sup> with an overall amount of 1.2 Li<sup>+</sup>. However, the biggest difference lies in the existence of quinone. A discharge plateau near 2.7 V is visible in the quinone-containing (MIL-53(Fe)<sub>y</sub>–quinone<sub>y</sub>) electrode, which is owing to the quinone reduction, and this phenomenon does not exist in quinone-free (MIL-53(Fe)) electrode. Unfortunately, the extra capacity relative to guest molecules attenuates during cycling, while the method of an electrochemically active guest molecules/MOF paves a new path toward establishing a classical electrolytes with ranking stability for LIBs.

In a word, the strategies to construct pristine MOFs by adopting functional metal center or mixed metal or organic linkers with redox activity or reactive activity are effective for the improvement of the conductivity and electrocatalytic activity of target MOFs. However, the pursuit of rational design for pristine MOFs with desired electrochemical performance still has formidable challenges up to date. The lack of further understanding about the mechanism of formation still

exists for MOFs with different functional linkers. Isorecticular expansion, topology-guided design, post-synthetic modification, and functional clusters as cores can realize the ideal fabrication of target MOFs to some extent, especially for highly stable MOFs.

## 2.2. MOF Composites for Electrochemical Applications

It is well known that MOFs are constructed by metal ions and organic ligands, so their applications can be implemented by altering the metal units and functionalization of the organic linker. Above-discussed various pristine MOFs display various electrochemical performances, which are due to the active metal centers and organic linkers. Furthermore, their unique pores are able to provide favorable space/channels for electrochemical reaction and ion/proton transfer and storage in the electrochemical applications. These applications are feasible but subject to some serious limitations based on the consideration of their conductivities and structural integrities upon redox changes, because most organic ligands and metal nodes used in MOF synthesis are not redox active and do not facilitate electron transfer. The integration of MOFs and functional species or matrices not only improves the present functions but also broadens the applications of MOFs. To enhance the electrical conductivity and extend the applications of MOFs, various MOF composites were fabricated including S@MOF, metal materials@MOF, carbon materials@MOF, and MOF deposited on conductive plate.

### 2.2.1. S@MOF Composites for Li-Based Batteries

The rechargeable LIB is quite popular as an electrochemical energy conversion apparatus, which has achieved a great commercial success as portable electronic devices owing to its high energy density. The anode and cathode of a typical LIB contain two redox couples.<sup>[226]</sup> For example, graphite and lithium cobalt oxide (LiCoO<sub>2</sub>) are typical anode and cathode materials with the capacities of 372 and 148 mA h g<sup>-1</sup>, respectively. In such a cell, Li<sup>+</sup> moves from the cathode (LiCoO<sub>2</sub>) to anode (graphite) through Li<sup>+</sup>-conducting electrolyte during the charging process. Li intercalation/alloy in the anode material is oxidized to Li<sup>+</sup>, then lithium ions move to the cathode (positive electrode) during discharging. Due to the limitation of energy and power density, the current LIBs still cannot fulfill the power requirement of electric vehicles. As a result, it is very crucial to develop electrodes and electrolyte of LIBs to improve their performance as well as to develop the next-generation Li-based batteries. Lithium-sulfur (Li-S) batteries are thought to be a promising candidate for next-generation battery owing to the high theoretical capacity of 1675 mA h g<sup>-1</sup> and the specific energy density of 2500 W h kg<sup>-1</sup>, environmental benignity, and low cost.<sup>[227]</sup> MOF composites provide an exciting opportunity to develop the electrode and electrolyte materials in LIBs<sup>[138-142]</sup> and Li-S batteries.<sup>[143-151]</sup>

For Li-S batteries, its drawbacks include the formation of soluble polysulfide from reduction, and the addition of conductive additives. In particular, the soluble polysulfide tends to

separate from the electrode. To tackle this issue, MIL-100(Cr), HKUST-1, MIL-53(Al), and zeolite-type MOF (ZIF-8) have been used as host materials for sulfur impregnation. MOF electrodes with sulfur inside its cavities have been found to remarkably increase the capacity retention and cycle life of Li-S cathodes.

Sulfur was embedded into the pores of MIL-100(Cr) to form MIL-100(Cr)@S-155 composite by the heat treatment at 155 °C.<sup>[143]</sup> The composite exhibited reversible capture and release of the polysulfides from the cavities of MOF during cycling for Li-S battery. Transmission electron microscopy and XPS revealed a weak binding between the polysulfides and MOF. Therefore, the MOF pore surfaces also exerted a significant influence on the cycle property. Mesoporous carbon/S and SBA-15/S composites were prepared so as to get further understanding of the mechanism of MIL-100(Cr)@S (**Figure 6**). The results verified that metal center (Cr), pore size, pore surface, as well as pore wall thickness exerted a synergetic effect on the Li-S battery.

A larger quantity of sulfur (40 wt%) was added to HKUST-1 to fabricate HKUST-1@S composite by Wang et al.<sup>[144]</sup> A high capacity for the HKUST-1@S-based battery can be observed with about 500 mA h g<sup>-1</sup> after 170 cycles. When the sulfur was confined into HKUST-1 framework, HKUST-1@S composite cathode exhibited the superior electrochemical performance. All experimental results from charge/discharge curves, CV, and the X-ray crystal structure demonstrated that a little part of sulfur confined inside the cavities existed in the state of S<sub>8</sub>, while a large quantity of S<sub>2</sub> and S<sub>4</sub> molecules provided such excellent battery performance. In HKUST-1@S composite cathode, the confinement effect of MOF slowed the release of sulfur from the electrolyte, which is associated with the interactions of sulfur molecules and open Cu<sup>2+</sup> sites on the basis of the XPS investigations.

In addition, a porous ZIF-8 particle was also selected as the host (**Figure 7**) for the storage of sulfur and suppression of the release of polysulfides, as it was expected to achieve a stable cycling by affinity with polysulfide anions for Li-S battery. For Li-S batteries, porous MOFs as host are applied. Zhou et al. found that ZIF-8/S composite exhibited impressively long cycle life over 300 cycles at 0.5 current rate (C) with slight decay of only 0.08% per cycle.<sup>[146]</sup> The electrode loading of 30 wt% sulfur exhibited outstanding discharge capacities of 1055 mA h g<sup>-1</sup> (based on sulfur) at 0.1C and 710 mA h g<sup>-1</sup> at 1C in an electrolyte with a low viscosity and high polysulfide solubility. Furthermore, the particle size of the host also plays a significant role. They systematically discussed the effect of particle size of ZIF-8 (from <20 nm to >1 μm) on electrochemical performance of Li-S batteries.<sup>[147]</sup> It is shown that when the particle size of ZIF-8 decreases, the utilization of sulfur increases and the best cycling stability can be achieved with a moderate size (200 nm) with 75% over 250 cycles at 0.5C. As expected, MOFs featuring open metal centers with Lewis acidity have strong interaction with the electronegative polysulfide anions, impelling capacity retention to a large extent. Xiao and co-workers have synthesized a new Ni-MOF, Ni<sub>6</sub>(BTB)<sub>4</sub>(BP)<sub>3</sub> (BP: 4,4'-bipyridyl), in which Ni(II) acts as Lewis acidic sites.<sup>[151]</sup> The Ni-MOF contains interwoven pore with mesopores of ≈2.8 nm and micropores of ≈1.4 nm, which can evidently immobilize polysulfides through physical and chemical interactions at molecular level, thus

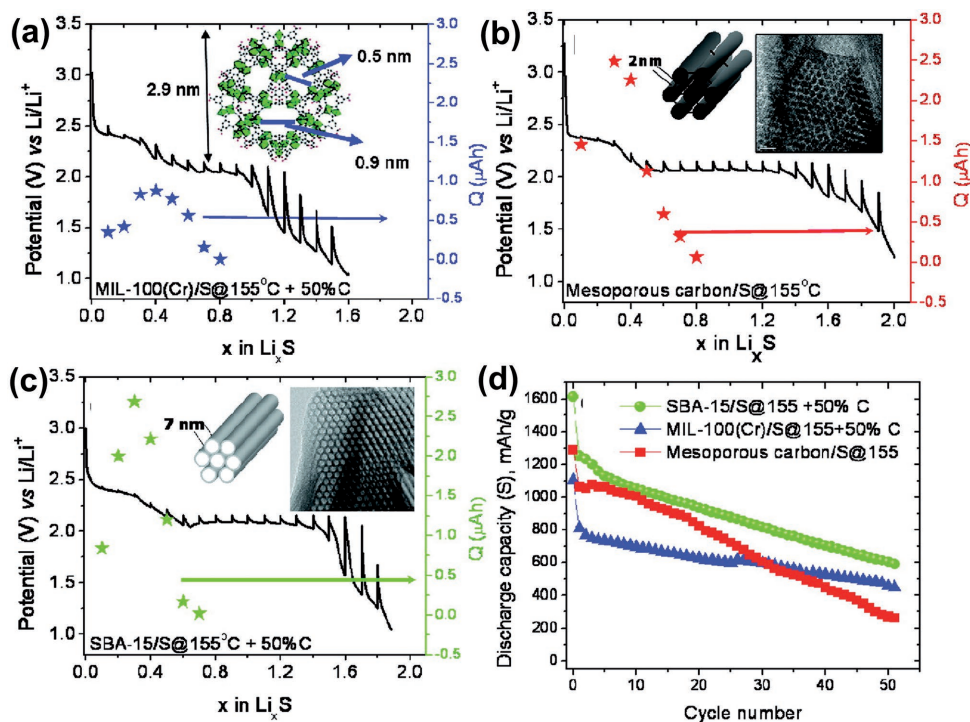


**Figure 6.** Electrochemical performance during the first reduction process of a) MIL-100(Cr)/S@155 °C + 50% C composite, b) mesoporous carbon/sulfur@155 °C, and c) SBA-15/S@155 °C + 50% C composite in LiTFSI (1 m) and tetramethylene sulfone (TMS) electrolyte with C/20 current density for the voltage range between 1.0 and 3.0 V vs Li. d) Cycling behavior of the composites in 1 m of LiTFSI in TMS electrolyte with C/10 current density for the voltage range between 1.0 and 3.0 V vs Li. Reproduced with permission.<sup>[143]</sup> Copyright 2011, American Chemical Society.

leading to an excellent cycling performance. The capacity retention can reach 89% after 100 cycles at 0.1C.

In short, during the past few years, a large variety of examples have been reported to incorporate a series of metals inside the cavities of MOF into metal@MOF composites, such as Pt, Cu, Ag, Ru, Au, and Pd. Such composites possess great potential for the development of heterogeneous catalysis. In 2010, Fischer and co-workers provided a very good review,<sup>[152]</sup>

where they systematically summarized the cases reported, in which metal nanoparticles were supported by or embedded into MOFs, as well as the major problems related to these novel nanocomposites. Among these composites, MOFs used as electrochemically active materials are still staying in the primary stage on account of their limited conductivity, large steric hindrance, and unmatched electrolyte. Here, we relate to metal including Fe, Co, Zn, Ag, Au, Pt, and Si; metal oxide including

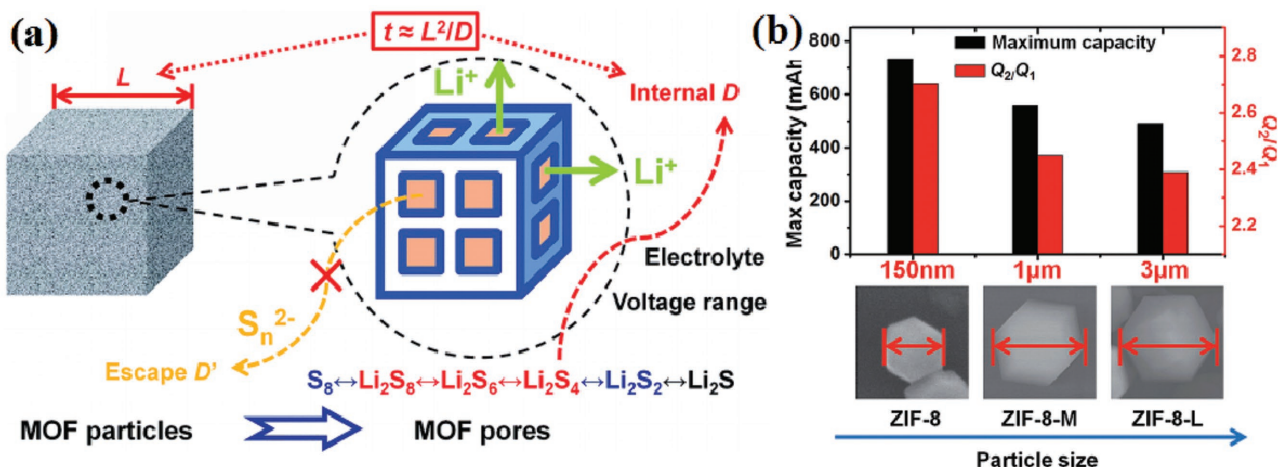


**Figure 7.** a) Factors of the rational design for a fast and stable cathode built from MOF and sulfur. b) Performances of S/ZIF-8 composites with different ZIF-8 particle sizes: the dependence of maximum discharge capacity and  $Q_2/Q_1$  on the particle size. Reproduced with permission.<sup>[146]</sup> Copyright 2014, Royal Society of Chemistry.



ZnO, Fe<sub>3</sub>O<sub>4</sub>, SnO<sub>2</sub>, MnO<sub>2</sub>, and CuO; metal salts including MoS<sub>x</sub>, Ni<sub>2</sub>(CO<sub>3</sub>)(OH)<sub>2</sub>, and the host MOF frameworks including MIL-53(Fe), ZIF-8, MIL-100(Cr), UiO-66, as well as a few new MOF structures.<sup>[153–170]</sup> As ordered porous materials, MOFs are fit for the uniform distribution of guests, which is very important, especially for nanometal catalysts.

### 2.2.2. Metal@MOF

Díaz et al. synthesized a Co8@MOF-5 composite (Zn<sub>3.68</sub>Co<sub>0.32</sub>O(BDC)<sub>3</sub>(DEF)<sub>0.75</sub>, (DEF: N,N-diethylformamide)) for the electrode of supercapacitor.<sup>[153]</sup> In this work, Zn centers in MOF-5 are partially substituted by Co into a bimetal composite. However, this Co8@MOF-5 is unsuitable for electrical conductor, since the capacitance is very low, so carbon black as additive material is added to enhance electrical conductivity. When electrochemically inactive MOF-5 was incorporated with Ag particles forming Ag@MOF-5(Zn),<sup>[154]</sup> its electrochemical behavior varied from “inactive” to “active.” Ag@MOF-5 for electrochemical oxidation of harmful pollutants, such as nitrophenols (2-methyl-4-nitrophenol, 4-nitrophenol, and 2-nitrophenol), can also be realized. Furthermore, enhanced electrochemical detection of nitrophenols was achieved by a modified GC electrode with the Ag@MOF-5(Zn) composite. When a Zn-doped Ni-MOF with layered structure was prepared by Wei and co-workers (Figure 8),<sup>[155]</sup> it exhibited large specific capacitances of 1620 and 854 F g<sup>-1</sup>, high rate capabilities of 0.25 and 10 A g<sup>-1</sup>, and good cycling stability, maintaining at over 91% of the retention even after 3000 cycles, which were higher than that of the

pure Ni-MOF. Such excellent performance can be ascribed to the layered structure and enlarged interlayer distance in Zn-doped Ni-MOF. Such pseudocapacitive behavior arises from the surface redox reactions, demonstrated by the CV curves with a couple of redox peaks, which may correspond to the intercalation and deintercalation of OH<sup>-</sup> during reactions, similar to the previous reports for Ni(OH)<sub>2</sub>.<sup>[228,229]</sup> Moreover, the increasing interlayer distance for the layered structure in Zn-doped Ni-MOF provides sufficient space for the electrolyte diffusion to ensure that the process of intercalation and deintercalation of OH<sup>-</sup> is more easier, leading to smaller charge transfer resistances and faster electron transfer rate during the charge–discharge process. Besides, the doped Zn<sup>2+</sup> acting as a pillar can effectively stabilize the skeleton of crystal during the cycling process.

Au (Au) NPs are, usually, used as an electrochemical sensing platform or catalyst. Recently, an Au NP@Cu-MOF composite has been synthesized by Rinaldi and co-workers based on a Cu-MOF,<sup>[156]</sup> nanowhisker of Al<sub>2</sub>O<sub>3</sub> silanized with (3-aminopropyl)triethoxysilane and Au NPs. CV behaviors of Au NP@MOF composite have approximately five times current density larger than the pristine MOF in 0.1 M phosphate buffer solution (PBS, pH 7.0) and 0.1 M KCl at the scan rate of 20 mV s<sup>-1</sup>. This material was prepared into an electrode in carbon paste (CPE), realizing the electrochemical sensing bisphenol A (BPA). Here, the CPE plays an important role in hindering MOF from degradation. Au NPs act with the MOF to enhance 2.5-fold signal output for BPA. In addition, Yadav et al. have verified that Au NP@MOF-5 material is also an effective electrocatalyst for oxidation of nitrite.<sup>[157]</sup> First, even in the presence of various

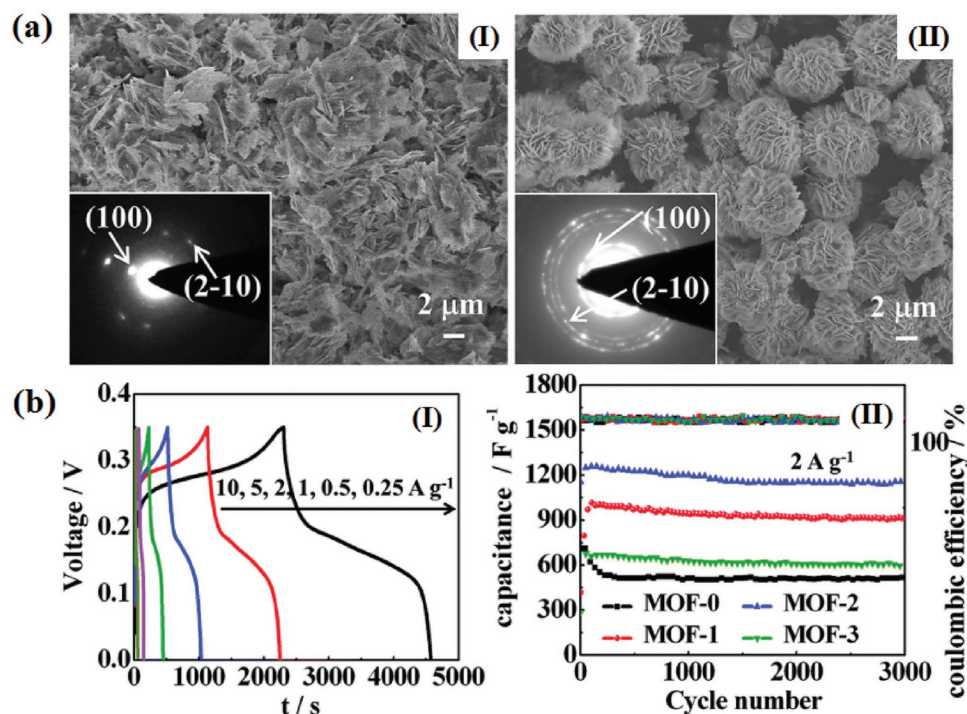


**Figure 8.** a) SEM images of Zn-doped Ni-MOF materials: I) MOF-0, II) MOF-2 (insets: the corresponding selected area electron diffraction (SAED) patterns). b) Electrochemical performances of Zn-doped Ni-MOF electrodes: I) charge–discharge profiles for MOF-2, II) galvanostatic charge–discharge (GCD) cycling performance. Reproduced with permission.<sup>[155]</sup> Copyright 2014, Royal Society of Chemistry.

interferences such as inorganic ions, phenols, and biological molecules, the Au NP@MOF-5 as an electrochemical sensing platform exhibits high stability and selectivity with a wide range of calibration. Its detection limit is  $1.0 \times 10^{-3}$  M with a sensitivity of  $0.23 \mu\text{A } \mu\text{M}^{-1} \text{cm}^{-2}$  for nitrite and  $15.3 \times 10^{-6}$  M with a sensitivity of  $0.43 \mu\text{A } \mu\text{M}^{-1} \text{cm}^{-2}$  for nitrobenzene. Furthermore, its electrocatalytic ability of nitrite oxidation and nitrobenzene reduction for Au NP@MOF-5 has also been realized based on measured CV responses in 0.1 M  $\text{N}_2$ -saturated PBS (pH 7.0) at  $20 \text{ mV s}^{-1}$  in the absence and presence of  $500 \times 10^{-3}$  M of nitrobenzene (NB).

It is well known that transition-metal complexes with Schiff-base ligands play an important role in oxygen transport and show high activity in the ORR, such as salen complexes. Thus, Cosalen@MIL-100(Cr) has been synthesized by inserting Co(II)-salen into MIL-100(Cr) pores.<sup>[158]</sup> The CV curve demonstrates that Cosalen@MIL-100(Cr) shows a well-defined reduction peak at  $-0.21$  V toward the ORR modified on GC electrode, indicating that this composite possesses an excellent electrocatalytic activity with a four-electron reduction pathway. These results suggest that the incorporation of Co(II)-salen into MOF remarkably enhances the electrocatalytic activity.

### 2.2.3. Metal Oxides@MOF

Similar to metal particles, some transition-metal macrocycles, metal oxides, and metal nitrides are also used as the electrocatalysts. Manganese oxides are considered as promising alternatives instead of Pt-based catalysts because of their excellent ORR catalytic activities, environmental compatibilities, and low cost.  $\text{MnO}_2$ @FeBTC composite was synthesized by integrating  $\epsilon$ - $\text{MnO}_2$  and an FeBTC MOF support.<sup>[159]</sup> Even though  $\text{MnO}_2$  has widely been used as an ORR catalyst in last several years, its ORR catalytic activities are restricted by agglomeration of particles during the reaction. When  $\epsilon$ - $\text{MnO}_2$  is inserted into the FeBTC framework,  $\epsilon$ - $\text{MnO}_2$  forms nanorods, with one end protruding and another firmly immobilized onto the FeBTC framework to effectively prevent the agglomeration. Thus, the composite displays superior ORR activity compared with  $\epsilon$ - $\text{MnO}_2$  and  $\text{MOF}(\text{Fe}) + \epsilon$ - $\text{MnO}_2$  in alkaline solution, which is similar to that of 20% Pt/C. An obvious four-electron transfer occurs during the ORR process of the  $\epsilon$ - $\text{MnO}_2$ @FeBTC composite, where  $\text{O}_2$  is first reduced to  $\text{H}_2\text{O}_2$ , followed by chemical decomposition to form primarily  $\text{OH}^-$  and  $\text{O}_2$ . The characteristic of high specific surface area in the FeBTC MOF with micropores aids oxygen diffusion, contributing to a superior ORR catalytic activity.

$\text{SnO}_2$  as electrode materials for supercapacitors has drawn great attention because of its chemical stability, as well as optical and electrical properties. Particularly,  $\text{SnO}_2$  quantum dots, due to their electric double layer capacitance, exhibit very obvious

oxidation–reduction peaks, which indicate that Faradaic reactions take place. As a typical MOF, ZIF-8 exhibits ultrastability even in organic solvents and boiling alkaline water. Tang and co-workers have dispersed  $\text{SnO}_2$  quantum dots into a ZIF-8 framework into  $\text{SnO}_2$  quantum dots@ZIF-8 composite by a simple in situ epoxide precipitation method.<sup>[160]</sup> Based on the electrochemical tests,  $\text{SnO}_2$  quantum dots@ZIF-8 material shows an excellent performance with a high capacitance of  $931 \text{ F g}^{-1}$  at  $5 \text{ mV s}^{-1}$  in 6 M KOH electrolyte. This result is much higher than  $\text{SnO}_2$  quantum dots ( $241 \text{ F g}^{-1}$ ) and ZIF-8 ( $99 \text{ F g}^{-1}$ ). The combination of ZIF-8 with a porous structure and  $\text{SnO}_2$  quantum dots maximizes the utilization of active material. Meanwhile, this composite shows a good cycling stability over 500 cycles. A novel  $\text{Cu}_x\text{O}$  nanoparticle@zeolitic imidazolate framework ( $\text{Cu}_x\text{O}$  NP@ZIF-8) was also fabricated with ZIF-8 as host (Figure 9).<sup>[161]</sup> Their synthesis is interesting that this composite  $\text{Cu}_x\text{O}$  NP@ZIF-8 is from the facile pyrolysis of HKUST-1@ZIF-8 nanocrystal based on the different thermal stability of the two MOFs, where HKUST-1 is converted into  $\text{Cu}_x\text{O}$  NPs, uniformly dispersing inside the host materials of ZIF-8, because ZIF-8 can remain its original structure under the same pyrolysis temperature. As an electrochemical sensor, this material realizes the detection of  $\text{H}_2\text{O}_2$  with a wide detection range from 1.5 to  $21\,442 \times 10^{-6}$  M, with high detection sensitivity ( $0.15 \times 10^{-6}$  M). Such performance arises from the synergistic effect of good electrocatalysis of  $\text{Cu}_x\text{O}$  NPs, and the proper pore shape and pore size for ZIF-8.

Semiconductive ZnO nanoparticles can be embedded into the cavities of ZIF-8 to prepare ZnO@ZIF-8 composite for electrochemical response.<sup>[162]</sup> A simple self-template strategy was developed by Zhan et al. for the fabrication of metal oxide semiconductor@MOF core–shell heterostructures with free-standing ZnO@ZIF-8 nanorods and vertically standing arrays (Figure 10). During the synthesis, ZnO nanorods act as the

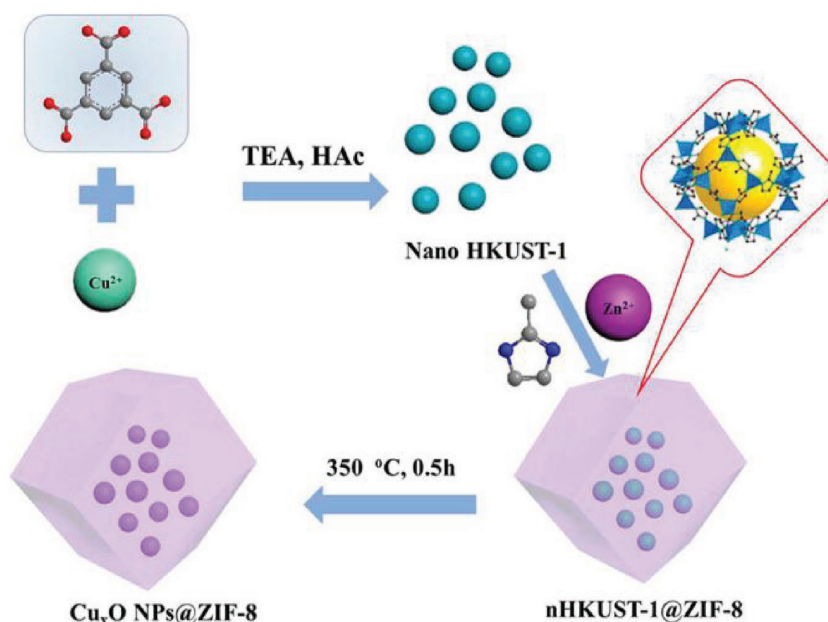


**Figure 9.** Schematic diagram of the construction of  $\text{Cu}_x\text{O}$  NP@ZIF-8. Reproduced with permission.<sup>[161]</sup> Copyright 2016, American Chemical Society.

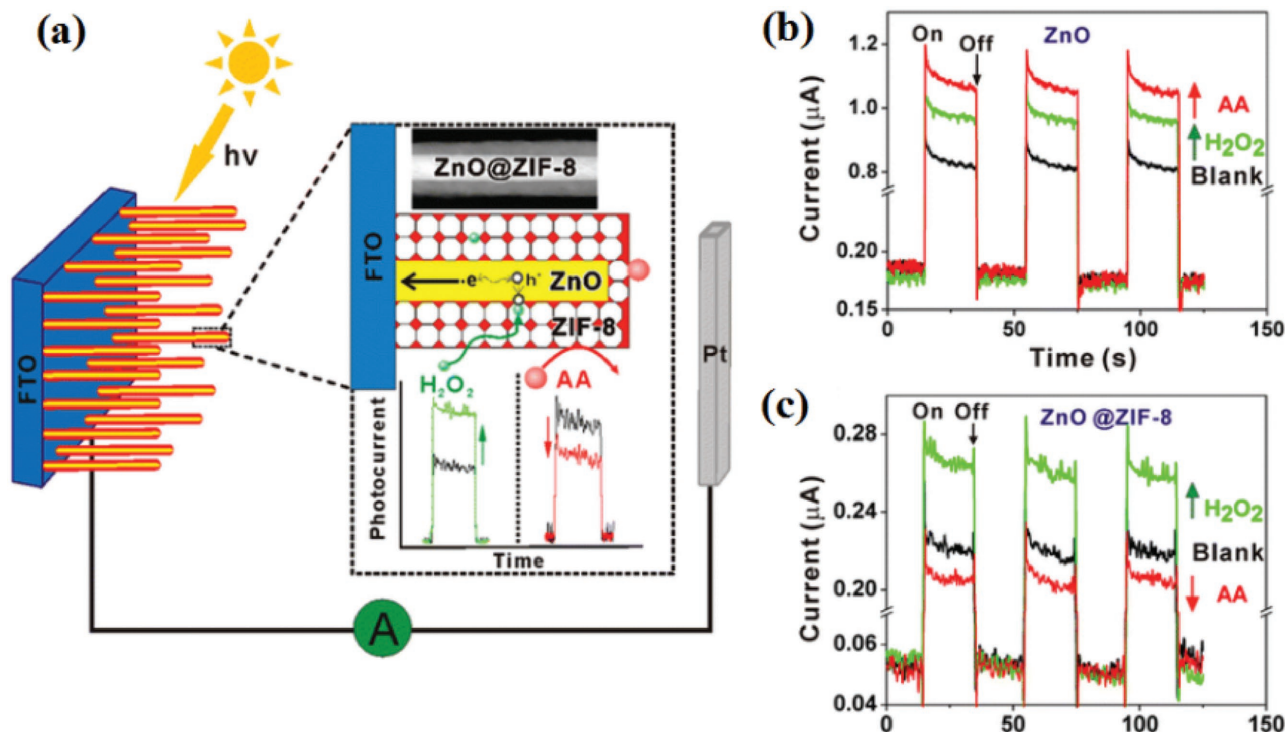


**Figure 10.** a) Schematic diagram of the photoelectrochemical (PEC) sensor with selectivity to  $\text{H}_2\text{O}_2$ . b) Photocurrent response of ZnO nanorod arrays against  $\text{H}_2\text{O}_2$  ( $0.1 \times 10^{-3} \text{ M}$ ) and ascorbic acid (AA) ( $0.1 \times 10^{-3} \text{ M}$ ). c) Photocurrent responses of the ZnO@ZIF-8 nanorod array in the presence of  $\text{H}_2\text{O}_2$  ( $0.1 \times 10^{-3} \text{ M}$ ) and AA ( $0.1 \times 10^{-3} \text{ M}$ ). Reproduced with permission.<sup>[162]</sup> Copyright 2013, American Chemical Society.

template and  $\text{Zn}^{2+}$  source for the growth of ZIF-8. It is well known that the detection of  $\text{H}_2\text{O}_2$  in a biosystem is very necessary, because overproduction of  $\text{H}_2\text{O}_2$  can cause disease-related pathophysiological complications in many conditions. The as-synthesized ZnO@ZIF-8 nanorod arrays exhibit obvious photoelectrochemical sensing response to  $\text{H}_2\text{O}_2$  with the existence of serous buffer solution. Besides, such a MOF composite with multifunctional core-shell heterostructures exhibits exciting catalytic abilities in electrochemical catalysis, which can be ascribed to the molecule-size-selective ability of the MOF shell.

#### 2.2.4. Metal Salts@MOF

Except for some metal and semiconductor metal oxide nanoparticles in the cavities of MOFs, the metal salts as conductive substrate can also improve the electrochemical activity. Over the past decades, compared with other transition-metal oxides, Ni-based materials as pseudocapacitor electrode materials, such as nickel oxides/hydroxides featuring outstanding redox activity and low cost, have received widespread attention due to their high theoretical specific capacitance of  $2082 \text{ F g}^{-1}$  within  $0.5 \text{ V}$ .<sup>[230–232]</sup> However, some drawbacks such as poor electrical conductivity and low surface limit their practical applications. The specific characteristics of porosity of MOFs just make up the shortcomings of nickel hydroxide. During electrochemical reactions, the electrolyte can penetrate into and move out of the MOF pores. Tang and co-workers have introduced  $\text{Ni}_2\text{CO}_3(\text{OH})_2$  into ZIF-8 cavities to form  $\text{Ni}_2\text{CO}_3(\text{OH})_2/\text{ZIF-8}$  composite as

the supercapacitor electrodes,<sup>[163]</sup> in which  $\text{Ni}_2\text{CO}_3(\text{OH})_2$  maximizes the utilization of active material, yielding a high specific capacitance. The  $\text{Ni}_2\text{CO}_3(\text{OH})_2/\text{ZIF-8}$  exhibits a specific capacitance of  $851 \text{ F g}^{-1}$  at  $5 \text{ mV s}^{-1}$  and good stability over 5000 cycles. The specific capacitance is superior to that of the pure ZIF-8 ( $140 \text{ F g}^{-1}$ ) and  $\text{Ni}_2\text{CO}_3(\text{OH})_2$  ( $668 \text{ F g}^{-1}$ ). UiO-66 was selected as host due to its excellent thermal stability (up to  $773 \text{ K}$ ) and high surface areas. They used UiO-66 (Zr(BTC) MOF) as the support and  $\text{Ni}_3(\text{NO}_3)_3(\text{OH})_4$  as an active material to prepare another  $\text{Ni}_3(\text{NO}_3)_2(\text{OH})_4/\text{Zr-MOF}$  composite for supercapacitors.<sup>[165]</sup> The porous structure of UiO-66 is beneficial to the insertion of the active material  $\text{Ni}_3(\text{NO}_3)_2(\text{OH})_4$  and interfacial charge transport. Besides, it also provides short diffusion channels for ions, forming a high specific capacitance. The as-prepared  $\text{Ni}_3(\text{NO}_3)_2(\text{OH})_4/\text{UiO-66}$  composite shows a large SC of  $992 \text{ F g}^{-1}$  at  $5 \text{ mV s}^{-1}$  in  $6 \text{ M KOH}$  because of the redox reactions on the electrode exterior, which is much higher than UiO-66 ( $\approx 134 \text{ F g}^{-1}$ ) and  $\text{Ni}_3(\text{NO}_3)_2(\text{OH})_4$  ( $\approx 753 \text{ F g}^{-1}$ ). With the increased scan rate, the capacitance decreases owing to limited ion diffusion rate to maintain the charge conservation during the oxidation–reduction reaction, and the inner active sites cannot completely keep their redox transitions at higher scan rates. It is mentioned that the largest SC values of the  $\text{Ni}_3(\text{NO}_3)_2(\text{OH})_4/\text{Zr-MOF}$  still retain a high capacitance of  $616 \text{ F g}^{-1}$  even after 3000 cycles, suggesting a relatively high stability of the composite.

Additionally, Dai et al. obtained a  $\text{MoS}_x/\text{Zr-MOF}$  composite by molybdenum polysulfide ( $\text{MoS}_x$ ) anchored on a porous Zr-MOF ( $\text{UiO-66-NH}_2$ ).<sup>[168]</sup> This composite exhibits remarkable



electrochemical activity for HER with a lower onset potential of nearly 125 mV, a overpotential of 200 mV at 10 mA cm<sup>-2</sup>, and a Tafel slope of 59 mV dec<sup>-1</sup>. Thus, it also displays excellent durability in an acid medium. Electrochemical impedance spectroscopy analyzed the mechanism of HER at the MoS<sub>x</sub>@Zr-MOF composite, in which the electron transports fast from the less conducting MoS<sub>x</sub> nanosheets to the electrode.

As described above, various metallic materials can be introduced into MOF pores for the synthesis MOF composites, which can significantly surpass the electrochemical activity of pristine MOFs. Nevertheless, most transition metals are unstable in acid media due to their corrosion. In this regard, the MOF@C composite is fabricated with various carbon materials (e.g., graphene, CNTs, carbon black, and hollow or porous carbon)<sup>[171–197]</sup> or some polymeric materials (e.g., polyaniline (PANI) and polypyrrole) adopted into MOFs.<sup>[198–205]</sup> This C family has been studied for the electrode and catalyst supports ascribed to their high specific surface area, high conductivity, and effective charge transfer at the electrodes.

### 2.2.5. GO@MOF

Graphene, a 2D single-atom-thick carbon material with a honeycomb lattice, has aroused tremendous attention for its application in energy conversion and storage with many favorable advantages,<sup>[233–238]</sup> such as outstanding electroconductivity, porous structure with light weight and high surface area, which can buffer the volumetric change to effectively reduce the crushing of active materials,<sup>[239,240]</sup> and the flexibility and mechanical strength. Generally, its oxidation state, graphene oxide (GO), always has some functional sites and groups.

HKUST-1 (Cu(BTC) MOF) was selected as host to construct MOF/GO composite.<sup>[171]</sup> Gao and co-workers found that MOF/GO hybrid material exhibits enhanced electrocatalytic performance toward dimethyl carbonate. Various measurements of the composite demonstrated that MOF/GO was effective for the electrolytic reaction with cycles for at least five times. Based on the catalyst, CO can be converted into dimethyl carbonate at normal temperature and pressure. The electrocatalytic mechanism was studied, and a plausible Cu(II)/Cu(I) cycle was put forward. From the result of the AC impedance spectroscopy, the MOF/GO hybrid shows smaller Faradic impedance in comparison with MOF alone, and its increasing conductivity suggests that the introduction of GO improves the composite's electron transfer ability.

Sawangphruk and co-workers synthesized a composite of 10 wt% rGO/HKUST-1 (rGO: reduced graphene oxide) with a large BET surface area of 1241 m<sup>2</sup> g<sup>-1</sup> and a specific pore volume of 0.78 cm<sup>3</sup> g<sup>-1</sup>.<sup>[172]</sup> Then, the composite fabricated on flexible carbon fiber paper exhibits a fivefold higher specific capacitance (385 F g<sup>-1</sup>) at an current density of 1 A g<sup>-1</sup> than that of the agglomerated rGO. In addition, its flexible solid-type supercapacitor offers a potential window of ≈1.6 V, and a high specific capacity (≈193 F g<sup>-1</sup>) can be observed over a continuous testing of 60 000 s with high capacity retention of 98% for 2000 cycles. The symmetric solid-type supercapacitor of the as-fabricated 1.8 in. × 4 in. supercapacitor exhibits a specific power (3100 W kg<sup>-1</sup>) and a specific energy (42 W h kg<sup>-1</sup>), which

can supply electricity to a spinning 3 V motor over 9 min discharging time. This strongly suggests that the composite can be utilized for flexible supercapacitor device.

Mobin and co-workers used the Cu-MOF/rGO hybrid to realize a multitasking for supercapacitor and electrochemical sensor (Figure 11).<sup>[173]</sup> The Cu-MOF/rGO hybrid is a high-performance material for the supercapacitors with large charge capacitance (685.33 F g<sup>-1</sup> at 1.6 A g<sup>-1</sup>), high energy (137.066 W h kg<sup>-1</sup>), enhanced power density (4800.04 W kg<sup>-1</sup>), and excellent rate ability (retaining 71.01% of initial capacitance at 8 A g<sup>-1</sup>). The capacitance of Cu-MOF/rGO/GCE is remarkably enhanced compared with that of the rest of electrodes (rGO/GCE, Cu-MOF/GCE) with various scan rates (10–500 mV s<sup>-1</sup>) due to perfect synergy between Cu-MOF crystals and wrinkled rGO nanosheets. The electrodes also show high stability with a long cycle life (91.91% after 1000 cycles). In addition, it displayed a remarkable sensitive response towards nitrite in a wide dynamic linear range of 3–40 000 × 10<sup>-6</sup> M (R<sup>2</sup> = 0.99911)

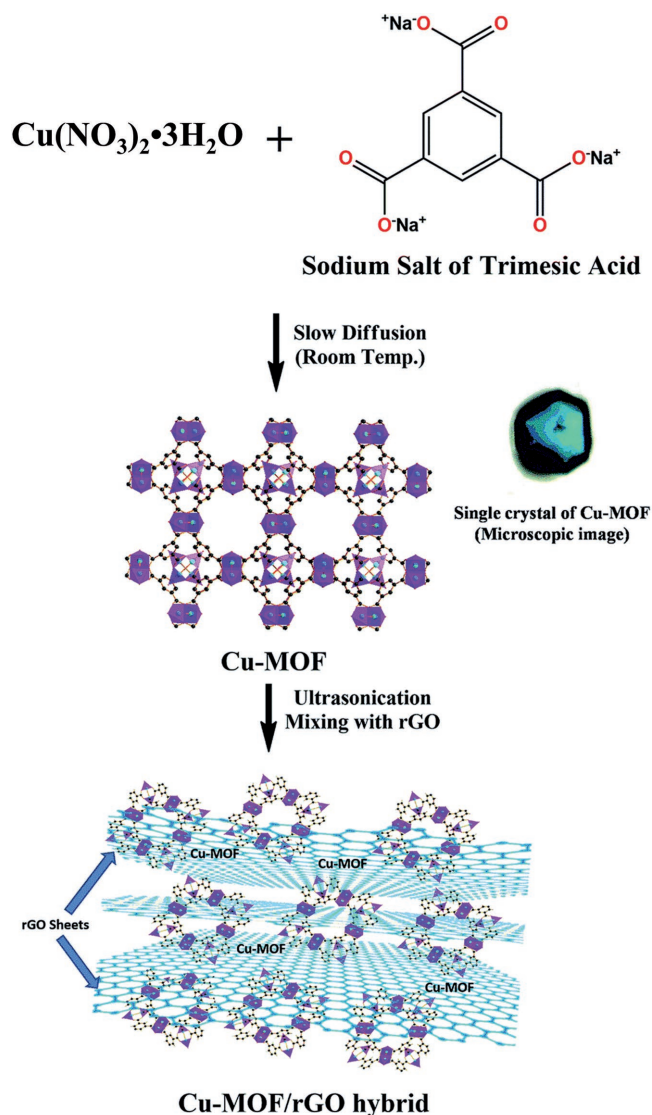


**Figure 11.** Schematic synthesis of the Cu-MOF/rGO hybrid. Reproduced with permission.<sup>[173]</sup> Copyright 2016, Royal Society of Chemistry.

featuring a notable detection limit of 33 nm, an excellent sensitivity of  $43.736 \mu\text{A} \mu\text{M}^{-1} \text{cm}^{-2}$ , and distinguished sensitivity in the presence of common interfering agents. The enhanced capacitance for Cu-MOF/rGO/GCE benefits from three factors: i) highly porous Cu-MOFs generate additional surface area and provide more channels for the charge transfer; ii) rGO was introduced along with the Cu-MOF to increase the conductivity; and iii) the presence of wrinkles on the crinkly rGO surface prevents restacking and markedly boosts up the conductivity by shortening the ion diffusion path.

Based on the similar mechanism, the as-constructed GO@Cu(BDC) MOF composite<sup>[174]</sup> showed good performance in HER, OER, and ORR. The power density of the composite accounts for 76% of that of the commercial Pt catalyst for the polymer electrolyte membrane fuel cell testing. Moreover, it displays high stability in acid due to the synergism of MOF and GO in the structure.

ZIF-8/GO nanocomposite was also prepared by Tang and co-workers via ultrasonication under the ambient condition.<sup>[175]</sup> The ZIF-8/GO nanocomposite in 6 M KOH electrolyte exhibits good pseudocapacitive behavior with a large specific capacitance of  $400 \text{ F g}^{-1}$  at  $10 \text{ mV s}^{-1}$  as well as good cyclicality, which is also applicable for the ZIF-67/GO. Both of them exhibit much higher than those of pristine MOFs, suggesting that the electrochemical performance of MOF materials can be improved by growing the ZIF nanocrystals on the exterior of GO.

Metalloporphyrin MOF (Fe-TCPP; TCPP: 5,10,15,20-tetrakis(4-carboxyl)-21H,23H-porphyrin) was fabricated into Fe-TCPP@GO composite by Loh and co-workers.<sup>[176]</sup> Fe porphyrins are very important for  $\text{O}_2$  transport and reduction reactions. The synthesis of the MOF composite was accomplished with the addition of pyridinium dye-functionalized rGO sheets to Fe-TCPP, presenting enhanced catalytic activity for ORR. The reason for this good electrochemical performance is as follows: first, by adding pyridine-functionalized graphene, the crystallization of MOF is altered, and the porosity and the rate of charge transfer of MOF also get enhanced. The synergistic effect of rGO and pyridinium linker makes the FeTCPP hybrid catalysts afford four-electron ORR transfer for promising application in Pt-free cathode in alkaline solutions. Compared with the Pt catalyst, this composite shows much higher ORR selectivity and an obviously reduced effect of methanol cross over.

In addition, GO@MOF composites not only improved the electrochemical activity of MOFs but also served as host material boosting the fixation of sulfur in Li-S batteries. Chen and co-workers discovered that graphene nanosheets (GNS)-wrapped Cr-MOF (MIL-101)/sulfur composite,<sup>[177]</sup> denoted as GNS-MIL-101(Cr)/S, possessed excellent immobilization capability for polysulfides and high electroconductivity with enhanced cycle stability and rate capability. Even the reversible capacity is  $809 \text{ mA h g}^{-1}$  after 134 cycles, the Coulombic efficiency keeps 96.6%, and capacity retention stays 95% at 0.8C. Based on a liquid-phase method, which was distinct from the synthesis method of MIL-101(Cr)/S, MIL-101(Cr)@rGO was prepared and used as the multicomposite sulfur cathode.<sup>[178]</sup> The discharge capacity of  $650 \text{ mA h g}^{-1}$  and capacity retention rate of 66.6% for MIL-101(Cr)@rGO/S composite sulfur cathode at the 50th cycle at the current density of  $335 \text{ mA g}^{-1}$

far exceed those of MIL-101(Cr)/S mixed cathode with the discharge capacity and capacity retention rate  $458 \text{ mA h g}^{-1}$  and 37.3%, respectively. Therefore, MIL-101(Cr)@rGO will be a promising candidate for cathode materials in Li-S batteries.

### 2.2.6. CNTs@MOF

As another member of carbon family, CNTs have numerous superiorities, including ultrasmall sizes, high electroconductibility, and chemical stability with tensile strength. Hence, CNTs also have wide applications in electronic devices and sensors. The introduction of CNTs into Mn-MOF ( $\text{Mn}(\text{C}_2\text{H}_3\text{O}_2)_2(\text{H}_2\text{O})_4$ ) can form CNTs@Mn-MOF composite,<sup>[179]</sup> thus resulting in the enhancement of electroconductibility and the specific capacitance from  $43.2 \text{ F g}^{-1}$  for pure Mn-MOF. Moreover, such a CNTs@Mn-MOF composite exhibits outstanding stability and power density, in which 88% retention capacitance of the initial one can be kept even after 3000 cycles. It can be seen that poor electroconductibility of the MOFs may be improved by introducing CNTs into the Mn-MOF.

SWCNTs@Cu-MOF-199 composite can be fabricated with SWCNTs and Cu-MOF-199 [Cu-MOF-199 =  $\text{Cu}_3(\text{BTC})_2$ ] for electrochemical sensing,<sup>[180]</sup> in which single-walled carbon nanotubes (SWCNTs) was first cast the bare GC electrode, then Cu-MOF-199 was electrodeposited on SWCNTs' modified electrode. With the synergy of SWCNTs and Cu-MOF-199, the composite not only exhibits an excellent electrocatalytic activity toward the oxidation of hydroquinone and catechol with good reproducibility, but also shows very low detection limits of 0.08 and  $0.1 \text{ mmol L}^{-1}$ , separately. Cu-bipy-BTC/MWCNTs composite (bipy: 2,2'-bipyridine) was also synthesized by immobilizing Cu-bipy-BTC on multiwalled carbon nanotubes (MWCNTs).<sup>[181]</sup> Then, the composite was modified on the exterior of GCE into Cu-bipy-BTC/MWCNTs/GCE. The modified electrode had a good performance toward  $\text{H}_2\text{O}_2$  detection in a wide linear region of 3–70 and 70–30 000  $\text{mmol L}^{-1}$ . In addition, a low detection limit of  $0.46 \text{ mmol L}^{-1}$  can be obtained. The above-mentioned performance, along with the good stability and repeatability, may arise from the good electroconductibility of MWCNTs and high catalytic activity of Cu-bipy-BTC.

In addition, MOF-5/3D-KSC composite is also fabricated based on 3D kenaf-stem-derived porous carbon (KSC) and spherical porous MOF-5 microstructures.<sup>[182]</sup> The MOF-5/3D-KSC composites can be directly used for integrated MOF-5/3D-KSC electrodes and show much better detective performance for ascorbic acid (AA) than traditional enzyme-based sensors and non-enzymatic sensors with a low detection limit ( $0.24 \times 10^{-3} \text{ M}$ ) and good stability. Macroporous carbon (MPC) was also incorporated into nanosized and nanocrystalline cobalt-based MOF (Co-MOF) to prepare MPC@MOF composite, also greatly improving electrochemical activity of Co-MOF.<sup>[183]</sup>

### 2.2.7. PEO@MOF

As a new class of materials, similar to zeolites, MOFs are considered as promising templates for incorporating and loading nanoparticles with functions, owing to their long-range order,

the tunable dimensionality, and chemical tailoring channels and cavities. Such strategies can significantly improve the electrochemical activity of MOFs. However MOFs also display a size effect for incorporated guests. So the simplest method is that MOFs are directly deposited on the electrode or suitable electrolyte. In order to achieve the goal, numerous polymers have been examined.<sup>[241,242]</sup> The greatest attention has been paid to PEO-based electrolytes because of the appealing superiorities, including safety, excellent chemical stability, and low cost.<sup>[243]</sup> Unfortunately, the applications of polymer electrolyte systems (PEO–LiX) are hampered due to their low ionic conductivity of  $10^{-6}$  S cm<sup>-1</sup> at normal temperature. When the temperature is above 70 °C, PEO can exhibit considerable ionic conductivity, which limits its applications at ambient temperature. Therefore, plenty of efforts have been dedicated to improving the ionic conductivity of PEO-based electrolytes. The addition of a porous filler with Lewis acidic surface to form CPE will be an attractive way, since Lewis acidic surface properties can increase ionic conductivity, and porous structures with functional groups are helpful to stabilize the electrolyte/Li interface.

Mg-BTC, Cu-BDC, and Al-BTC MOF-incorporated CPEs, as well as poly(ethylene oxide)-based nanocomposite polymer electrolyte membranes have also been successfully prepared, which are composed of PEO and lithium bistrifluoromethane sulfonylimide (LiTFSI).<sup>[202–204]</sup> The ionic conductivity of CPE can be significantly enhanced two orders of magnitudes even at 0 °C through inserting MOF in the polymeric matrix. This method can also improve the thermal stability, compatibility, elongation at break of the polymeric membrane because the defective MOF frameworks play a critical role in improving the mobility of the Li<sup>+</sup> ion in the polymeric matrix. This all-solid-state lithium polymer cell made up of Li/CPE/LiFePO<sub>4</sub> has delivered a stable discharge capacity of 110 mA h g<sup>-1</sup> at 70 °C with a current rate of 1C.<sup>[203]</sup> These remarkable and appealing properties demonstrate that the MOF-incorporated nanocomposite polymer electrolytes are an effective strategy for enhancing conductivity.

MOF-5 was incorporated in PEO based CPE by Yuan et al. to improve its electrochemical property in LIB.<sup>[201]</sup> The composition of PEO–LiN(SO<sub>2</sub>CF<sub>3</sub>)<sub>2</sub>(EO (ethylene oxide):Li = 10:1)/10 wt% MOF-5 displayed a good ionic conductivity of  $3.16 \times 10^{-5}$  S cm<sup>-1</sup> at 25 °C. Moreover, the interfacial resistances of Li/CPE/Li cells upon storage were more stable than those without MOF-5. Besides, the capacity retention of 45% can be obtained after 100 cycles at 80 °C compared with the tremendous decay of the sample without the addition of MOF-5. Furthermore, they selected MIL-53(Al) to construct a PEO-based thin-film electrolyte.<sup>[205]</sup> Similar to MOF-5-incorporated PEO–CPE complex, MIL-53(Al) was selected as a filler and LiTFSI acted as the lithium source, a new PEO–MIL-53(Al)–LiTFSI thin electrolyte was fabricated. Based on this electrolyte, an all-solid-state LiFePO<sub>4</sub>/Li battery was fabricated. When analyzing the results of ionic conductivities for the thin film electrolyte with different amounts of EO, it can be found that the thin-film electrolyte shows the highest ionic conductivity of  $3.39 \times 10^{-3}$  S cm<sup>-1</sup> with a ratio of 15:1 (EO/Li), the MIL-53(Al) concentration of 10 wt%, which is much higher than  $9.66 \times 10^{-4}$  S cm<sup>-1</sup> without MIL-53(Al). In addition, the all-solid-state LiFePO<sub>4</sub>/PEO–MIL-53(Al)–LiTFSI/Li battery also exhibits better cycling performance than the ones

with PEO-based electrolyte reported at high rates and temperatures. At 5C (current rate) and 120 °C, its discharge capacity is 136.4 mA h g<sup>-1</sup> in the initial cycle, 129.2 mA h g<sup>-1</sup> in the 300th cycle, and 83.5 mA h g<sup>-1</sup> in the 1400th cycle, respectively. When the battery is cycled at 10C and 120 °C, its discharge capacity is 116.2 mA h g<sup>-1</sup> in the initial cycle and 103.5 mA h g<sup>-1</sup> in the 110th cycle. All of the results reveal that MOF-5 and MIL-53(Al) can not only modify the structure of the composite for charge transfer, but also improve the performance for solid LIB.

### 2.2.8. MOF-Deposited Conductive Plates

It can be found that it is an effective way to improve electrochemical activity and stability by fabricating the conductive substrates with MOF films. Considering the improved charge transfer of the fabricated electrodes, this strategy ensures the application of the substrates in photovoltaics, fuel cells, and sensors. Usually, the fabrication of MOF films onto the substrate contains charge driving, anodic dissolution, as well as cathode reduction. If the starting metallic materials come from electrodes, the same metal will be used for the anode and cathode. Different MOF thin films can also be successfully achieved with thicknesses from nanometers to micrometers, as well as low roughness or high homogeneity. These characteristics are very important for application-specific configurations, particularly in separation, electric devices, as well as sensors. Recently, Li et al. summarized the preparation, mechanism, and characterization techniques of the electrochemical deposit method for MOF thin films.<sup>[244]</sup> Three types of substrates were used for deposition of MOF thin films containing metallic substrates, conductive glass, and glassy carbon substrates. Qiu and co-workers discussed in detail the fabrication techniques of MOF membranes for the applications of gas and liquid separation.<sup>[20]</sup> Some typical synthesis strategies containing hydro/solvothermal methods, ultrasonication, a solvent evaporation diffusion, and microwave reaction, etc., can be utilized to fabricate MOF membranes, which have been demonstrated effective for the construction of zeolite membranes with similar porous structure. Generally, there are two methods: in situ direct growth and secondary (seeded-assisted) growth. The methods of direct growth contain growth on unmodified supports and on modified supports. However, the support materials for direct growth are very limited, so the secondary growth method is developed. For the seed-assisted growth method, the orientation is relatively easy to control, which is free from cracks or intercrystalline gaps. In addition, postsynthesis modification is also an effective method, which can adjust the structure of pores and interactions between the cavities and separation molecules by changing the internal surface of cages. However, the application of MOF thin films is closely dependent on the properties of substrate. Taking MOF thin film deposited on porous substrates as an example, if they are fabricated on signal transduction surfaces such as electronics, and microcantilevers the formed MOF thin film can be applied to chemical and physical sensing. When conductive supports are selected, such as metal plates, glass and glassy carbon, and ITO glass, the MOF thin film obtained will be effective for electrochemical applications. The electrochemical deposition method for constructing MOF



thin films has many advantages such as mild and fast preparation, simple scaling up, and regulation of morphology with voltage changes. In 2009, an electrochemical route was developed by De Vos and co-workers to grow HKUST-1 thin films on Cu plate.<sup>[245]</sup> First,  $\text{Cu}^{2+}$  ions were obtained by the oxidation of  $\text{Cu}(0)$  from Cu electrode under an anodic voltage. Second,  $\text{Cu}^{2+}$  ions reacted with BTC ligand in the reaction solution to form thin HKUST-1 film on the surface of the Cu anode. Except that MOFs can be fabricated into thin films, they can also be coated on various substrates. Recently, Worrall et al. have also fabricated different zeolitic imidazolate framework ZIFs on Zn and Co electrodes via the anodic dissolution method.<sup>[208]</sup> Electrochemical results showed that the areal capacitance of ZIF-67-free-coated Co electrodes was  $10.45 \text{ mF cm}^{-2}$  at  $0.01 \text{ V s}^{-1}$ , much higher than that of some MOF/GO composites. They also coated HKUST-1 on Cu electrode to study its redox-based data storage behavior. The electrolyte concentration and electrode separation result in “on”/“off” current densities of the order of  $1 \text{ mA cm}^{-2}$ , an “on”/“off” ratio of  $\approx 5$ , “on”/“off” states stability of at least ten consecutive reads, rewriteability over 6000 cycles, and the storage of data that can still be read hours after writing. Such data storage behavior is attributed to the immobilization of a fixed number of electrically accessible Cu cations within the porous HKUST-1 framework; hence, they are in the vicinity of the electrode surfaces and undergo facile redox conversion of  $\text{Cu}^{2+}$  and  $\text{Cu}^+$  as a function of the potential.<sup>[210]</sup>

Electroactive NENU-3 MOF, composed of  $\text{Cu}_3(\text{BTC})_2$  and Keggin-type heteropolyacid (phosphotungstic acid), can be coated on the copper electrode to form thin film,<sup>[212]</sup> and this film electrode presents excellent bromate reduction activity. In addition, bromate can also be detected in a wide linear range ( $0.05 \times 10^{-6}$  to  $72.74 \times 10^{-6} \text{ M}$ ) with a lower detection limit of  $12 \times 10^{-6} \text{ M}$ .

Another conductive polymer, PANI, was also utilized for interweaving MOF crystals by electrochemical deposition. For example, a flexible conductive porous electrode, namely, PANI-ZIF-67-CC, was obtained by electrodeposition of PANI after ZIF-67 growth on carbon cloth (CC) (Figure 12).<sup>[246]</sup> These PANI chains interconnect isolated MOF crystals as bridges for electron transportation between the external circuit and the internal surface of MOFs, which effectively enhance the conductivity of MOFs and facilitate Faradaic processes in the system. Hence, the as-prepared PANI-ZIF-67-CC displays an unprecedented high areal capacitance ( $2146 \text{ mF cm}^{-2}$ ) at  $10 \text{ mV s}^{-1}$  in a three-electrode system. Moreover, it yields a remarkable areal capacitance of  $35 \text{ mF cm}^{-2}$  and a high power density of  $0.833 \text{ W cm}^{-3}$  at  $0.05 \text{ mA cm}^{-2}$ , as well as over 80% capacitance retention after 2000 cycles.

### 2.2.9. LDH@MOF Composites

As a type of ionic lamellar compounds, LDHs,<sup>[247–249]</sup> with a general formula  $[\text{M}^{\text{II}}_{1-x}\text{M}^{\text{III}}_x(\text{OH})_2]^{x+}(\text{An}^-)_{x/n} \cdot y\text{H}_2\text{O}$  in which  $\text{M}^{2+}$  and  $\text{M}^{3+}$  stand for bivalent and trivalent metal cations, such as  $\text{Mg}^{2+}$ ,  $\text{Zn}^{2+}$ ,  $\text{Ni}^{2+}$ ,  $\text{Al}^{3+}$ ,  $\text{Ga}^{3+}$ ,  $\text{Fe}^{3+}$ , and  $\text{Mn}^{3+}$ , with  $x = 0.2–0.4$ ,  $\text{An}^-$  stands for inorganic or organic anion for charge compensation, e.g.,  $\text{Cl}^-$ ,  $\text{RCO}_2^-$ ,  $\text{CO}_3^{2-}$ , and  $\text{SO}_4^{2-}$ , consist of positively charged brucite-like layers. LDHs may also contain  $\text{M}^+$  and  $\text{M}^{4+}$  cations but these are fit for specific examples such as  $\text{Li}^+$  and  $\text{Ti}^{4+}$ , resulting in a variety of isostructural materials. LDHs have extensive applications as catalysts, ion exchange hosts, and drug delivery hosts, fire retardant additives, and cement additives. In particular, LDH is a 2D nanosheet with a thickness from around 1 nm to a sub-micrometer or several tens of micrometers. These properties allow them to serve as an ideal 2D

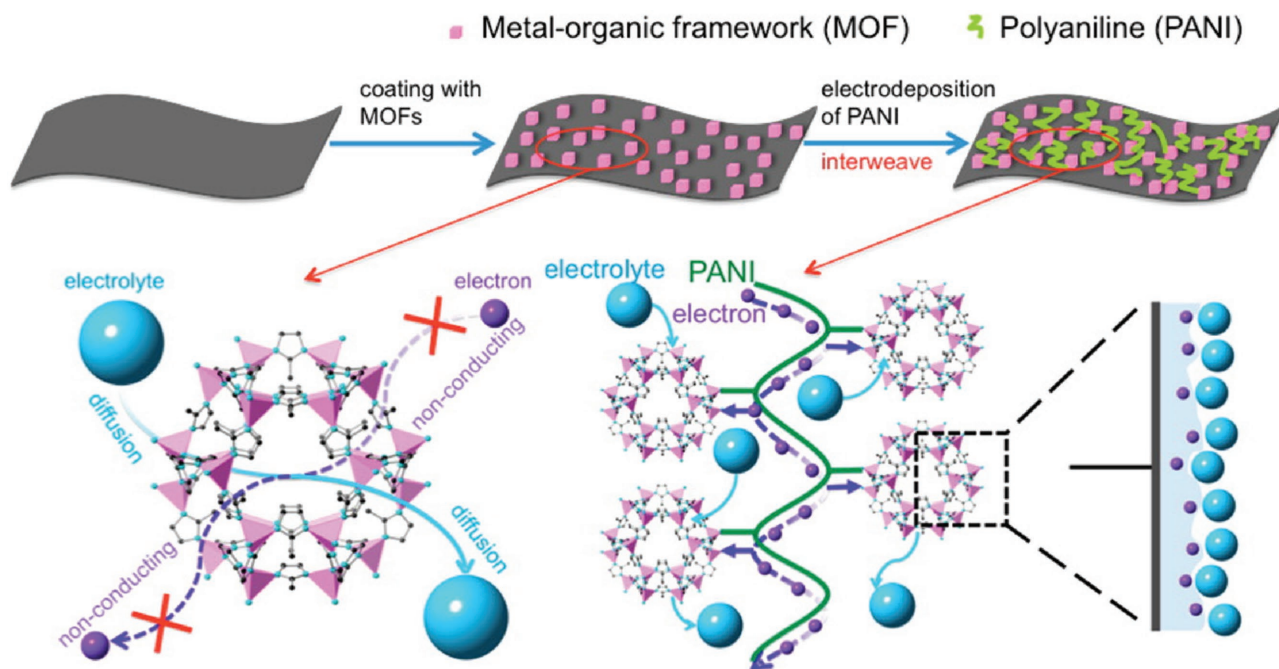


**Figure 12.** Schematic diagram for electron and electrolyte conduction in MOF and MOF interwoven by PANI. Reproduced with permission.<sup>[246]</sup> Copyright 2015, American Chemical Society.

quantum system to construct functional solid for their application in electronic and photonic devices. For example, LDHs can be constructed into symmetric supercapacitors to realize a further enhancement of energy and power density. Recently, Dou et al. have fabricated an LDH@ZIF-67 composite via a hydrothermal method, in which Ni substrate fabricated with LDH film was used for the growth of ZIF-67.<sup>[250]</sup> Then, the LDH@ZIF-67 was oxidized, carbonized, and sulfurized into hierarchically structured derivatives, MMO@Co<sub>3</sub>O<sub>4</sub>, spinelle@C, and LDH@CoS, respectively, with specific capacitances of 692, 781, and 1205 F g<sup>-1</sup> at 1 A g<sup>-1</sup>. Their hierarchical structures were kept in these derivatives with high surface area, which contributed to total capacitances because most exposed active species can participate in the charge and discharge process. Reversible ion accumulation at the interface can be reduced because of the synergistic effect from fast electronic transfer. In addition, rapid electron transfer can be realized through the combination of sulfides with excellent electroconductibility and the remarkable interaction between LDH and CoS. Therefore, LDH@CoS exhibits an excellent specific energy (44.5 W h kg<sup>-1</sup>) at the current density of 20 A g<sup>-1</sup> and good capacitance retention of 88.5% after 2000 cycles. The research demonstrated here is viable for the synthesis of LDH@MOF composites as supercapacitor components.

Compared with pristine MOFs, MOF composites have some own unique advantages, and MOF composites broaden the scope of application for MOFs. First, they can be fabricated based on the particular direction other than the random mixtures. Second, the combination of MOFs and functional materials exhibits synergistic effect, which will be superior to any one of individual components. Third, MOFs as host matrices can prevent aggregation and migration of nano-objects inserted to generate uniform distribution. Fourth, MOFs with different pore/channel sizes and cage-like pores are suitable supports to preserve leaching. Fifth, MOFs with hierarchical pores can act as a microreactor, which is one promising approach and has been taken advantage of in the field of separation, catalysis, and sensing. Sixth, the ordered crystal structures for formed MOF composite can be retained, which will be very useful to confirm the interaction between MOF framework and inserted molecules by some experimental tests, such as XRD and IR, and theoretical calculation. However, one question should not be ignored that the initial MOF structure may be destroyed during the formation of MOF composites. Hence, MOF composites are mainly based on a small number of classic MOF structures, such as ZIF family, HKUST-1, MIL, and IRMOF series in this case. For pristine MOFs and MOF composites, thermal as well as chemical stability is a key consideration for electrochemical application based on its acidic and alkaline testing condition. The functionality of MOFs is directly related to their textures. When MOFs are used for electrochemical testing, metal nodes and organic linkers are exposed to acidic/basic solution. In acidic solution, carboxylate groups are gradually protonated, which may explain the reason that most MOFs display higher stability in basic solution instead of acidic condition, especially for a large number of MOFs constructed by carboxylate ligands. Therefore, ZIF family exhibits relatively high stability. Based on this consideration, dual-functional ligands were widely adopted for the construction of MOFs containing carboxylate groups and

N-donor ligands. Based on the combination of electrochemical application, it may be an ideal recipe that Fe, Co, Ni, V, Mo, etc. with potential redox active are selected as metal centers, and dual-functional ligands are adopted as linkers, constructing pillared layered MOF framework, furthermore fabricating MOF composites.

### 3. Conclusion

MOFs have been explored for decades in the fields ranging from the synthesis of crystal structures to their application. By varying metal ions/organic linkers, along with the original versatile characters of MOFs including high surface area, controllable structure, ordered, meso- or microporous, and tunable pore, the specific characteristics of functional MOFs can be fully brought into many applications in the area of electrochemistry, such as LIBs and Li-S batteries, supercapacitor, proton conductor, electrocatalysis (HER, ORR, small organic molecules, or pollution molecules), electrochemical sensor. First, many efforts have been made to improve the conductivity of MOFs by a variety of methods, such as adopting metal center or mixed metal units with redox activity or organic linkers with reactive activity for pristine MOFs<sup>[84–135]</sup> or fabricating MOF composites<sup>[136–213]</sup> containing various conductive materials@MOF, such as metal, metal oxide, different carbon materials, LDH sheet, or conductive plates. Besides, MOF composites can be also fabricated through immersing MOFs into various solvents containing conductive materials through the ion-exchange method, where the immersing time will directly affect the amount of loading conductive materials and further decide the active sites for their electrochemical performances. Among these methods, the redox strategy is very efficient to improve conductivity of MOFs. Therefore, such a method could be extensively applied to the construction of diverse kinds of pristine MOFs or MOF composites based on polyvalent metal and plentiful ligands featuring reducing functional groups. In addition, many methods for improving the stability of MOFs have been described here. These approaches not only enhance the conductivity of MOF materials but also expand their applications in many other areas. However, a deeper understanding of synthetic strategy and relationship between synthesis and application is still a long-term direction for us to strive, as the electrochemical application of MOFs is at an early stage. In general, the future challenges to the researchers are five aspects: i) the precise control of pristine MOF structures, ii) the deep investigation of mechanism toward MOF structures with high conduction, iii) the effective fabrication for MOF of objective molecules, iv) the enhancement of stability, and v) the fabrication and practical application of MOF electrochemical devices.

- i) A precise control of the target structures for pristine MOFs remains difficult due to the limited understanding of self-assembly in a closed synthetic condition, for example, the effect of synthetic condition on increasing or decreasing the surface area and pore size of MOFs. It is urgently needed to clearly understand this issue, and very beneficial to design and construct suitable MOFs with regular or hierarchical pores, and adjustable composition and high surface area.

Electrochemical-application-oriented MOFs, especially those with hierarchical pores as electrochemical sensors or catalysts, can be obtained by multimetallic and mixed-ligand methods. Besides, various metal ions and ligands will be favorable for the fabrication of the backbones of MOFs for electrochemical application, as well as for improvement of the stability of the frameworks. In MOF composites, it may be relatively easily realized for application-based design by selecting MOF backbones and functional materials.

- ii) The understanding of the mechanism for MOF electrochemical application is of great significance for the synthesis of new function materials. Currently, only a few reports provide detailed explanation for the mechanism. The most important parameter of MOFs for their electrochemical application is conductivity. However, common MOFs possess low conductivity. Currently, the studies regarding the relationship between the electronic conductivity and structural property are scarce. To address this issue, a large number of MOF composites are needed to be fabricated by introducing conductive guest molecules. Additionally, some methods presented here can efficiently improve the conductivity of pristine MOFs, but it is still confusing about the effect of the main backbone on the conductive property. If MOFs are designed and constructed with high electrical conductivity, it will allow them to address an important and principal challenge associated with the electrochemistry.
- iii) The excellent electrochemical performance of MOF composites is mainly based on a large number of experiments and tests. Till now, a few reports in the literature have reported the effect of different kinds of functional guests on MOF backbones. Besides, the morphology, size, and dispersion of inserted particles and MOF hosts are very critical to synthesis and performance of MOF composites, which directly influence the interactions between hosts and guests. Therefore, MOF particles with functionalized surface and size-tunable matrices will be in great need. But the related research is still in its infancy.
- iv) The stability of materials is a primary factor for practical application. For the electrochemical application, chemical stability of materials in wide pH range is critical. The dual-ligand strategy with two different functions, such as combining carboxylate ligand and basic N-donor ligand, is proved to be successful, effective to enhance the stability of target MOFs, as discussed here. Such complementary ligands provide an additional level of control not only in desired MOF structure but also in charge density distributions. Except for several series of MOFs containing, e.g., ZIF family, Zr-MOFs, and MIL-101(Cr), the stability of other MOFs is hard to be predicted. The overall investigation on influence factor toward stability of MOFs still lacks a systematic study.
- v) The practical application in electrochemistry of pristine MOFs and MOF composites entails much effort, especially the preparation of MOF devices. MOFs exhibit some advantages in fabrication of electrochemical devices: i) metal nodes and organic ligands in a predetermined spatial orientation based on its topological prediction, ii) long-range order, and iii) synthetic flexibility. Over the past few years, several MOF membranes have been fabricated with

micro- or nanoscale devices, but it is not yet available for commercial tools. The difficulty focuses on the control of thickness, functionality, and a large scale for MOF films.

Here, we have done our utmost to provide a newest overview with current studies as much as possible. Nevertheless, it is difficult to take all publications into consideration due to limitation of space. We apologize here if some significant contributions are neglected.

## Acknowledgements

The authors are grateful to the editor for kind invitation and the reviewers for their valuable comments and constructive suggestions. F.-Y.Y. acknowledges the support by the K. C. Wong Magna Fund in Ningbo University and the Social Development Foundation of Ningbo (No. 2017A610065). H.-L.J. thanks the NSFC (21673213, 21371162, and 21521001), the 973 program (2014CB931803), and the Recruitment Program of Global Youth Experts. Q.X. thanks AIST, METI, and JSPS for financial support.

## Conflict of Interest

The authors declare no conflict of interest.

## Keywords

electrochemistry, metal-organic frameworks, MOF composites, synthesis strategies

Received: May 12, 2017

Revised: July 15, 2017

Published online: October 13, 2017

- [1] O. M. Yaghi, G. M. Li, H. L. Li, *Nature* **1995**, 378, 703.
- [2] B. F. Hoskins, R. Robson, *J. Am. Chem. Soc.* **1989**, 111, 5962.
- [3] B. F. Hoskins, R. Robson, *J. Am. Chem. Soc.* **1990**, 112, 1546.
- [4] D. Venkataraman, G. B. Gardner, S. Lee, J. S. Moore, *J. Am. Chem. Soc.* **1995**, 117, 11600.
- [5] G. B. Gardner, D. Venkataraman, J. S. Moore, S. Lee, *Nature* **1995**, 374, 792.
- [6] G. Férey, *Chem. Soc. Rev.* **2008**, 37, 191.
- [7] S. Horike, S. Shimomura, S. Kitagawa, *Nat. Chem.* **2009**, 1, 695.
- [8] H. Furukawa, K. E. Cordova, M. O'Keeffe, O. M. Yaghi, *Science* **2013**, 341, 974.
- [9] J.-P. Zhang, X.-M. Chen, *J. Am. Chem. Soc.* **2008**, 130, 6010.
- [10] J. R. Li, R. J. Kuppler, H. C. Zhou, *Chem. Soc. Rev.* **2009**, 38, 1477, and references therein.
- [11] M. P. Suh, H. J. Park, T. K. Prasad, D. W. Lim, *Chem. Rev.* **2012**, 112, 782, and references therein.
- [12] H. H. Wu, Q. H. Gong, D. H. Olson, J. Li, *Chem. Rev.* **2012**, 112, 836, and references therein.
- [13] S. H. Yang, X. Lin, W. Lewis, M. Suyetin, E. Bichoutskaia, J. E. Parker, C. C. Tang, D. R. Allan, P. J. Rizkallah, P. Hubberstey, N. R. Champness, K. M. Thomas, A. J. Blake, M. Schröder, *Nat. Mater.* **2012**, 11, 710.
- [14] P. Nugent, Y. Belmabkhout, S. D. Burd, A. J. Cairns, R. Luebke, K. Forrest, T. Pham, S. Ma, B. Space, L. Wojtas, M. Eddaoudi, M. J. Zaworotko, *Nature* **2013**, 495, 80.



- [15] Y. Peng, V. Krungleviciute, I. Eryazici, J. T. Hupp, O. K. Farha, T. Yildirim, *J. Am. Chem. Soc.* **2013**, *135*, 11887.
- [16] K. Sumida, D. L. Rogow, J. A. Mason, T. M. McDonald, E. D. Bloch, Z. R. Herm, T. H. Bae, J. R. Long, *Chem. Rev.* **2012**, *112*, 724.
- [17] Y. He, W. Zhou, G. Qian, B. Chen, *Chem. Soc. Rev.* **2014**, *43*, 5657.
- [18] J. R. Li, J. Sculley, H. C. Zhou, *Chem. Rev.* **2012**, *112*, 869.
- [19] B. Van de Voorde, B. Bueken, J. Denayer, D. De Vos, *Chem. Soc. Rev.* **2014**, *43*, 5766.
- [20] S. Qiu, M. Xue, G. Zhu, *Chem. Soc. Rev.* **2014**, *43*, 6116.
- [21] Q.-L. Zhu, Q. Xu, *Energy Environ. Sci.* **2015**, *8*, 478.
- [22] J. M. Yoon, R. Srirambalaji, K. Kim, *Chem. Rev.* **2012**, *112*, 1196, and references therein.
- [23] J. Liu, L. Chen, H. Cui, J. Zhang, L. Zhang, C.-Y. Su, *Chem. Soc. Rev.* **2014**, *43*, 6011.
- [24] G. Huang, Y.-Z. Chen, H.-L. Jiang, *Acta Chim. Sin.* **2016**, *74*, 113.
- [25] Y.-Z. Chen, Z. U. Wang, H. Wang, J. Lu, S.-H. Yu, H.-L. Jiang, *J. Am. Chem. Soc.* **2017**, *139*, 2035.
- [26] S. Ou, C.-D. Wu, *Inorg. Chem. Front.* **2014**, *1*, 721.
- [27] L. Zeng, X. Guo, C. He, C. Duan, *ACS Catal.* **2016**, *6*, 7935.
- [28] A. Aijaz, A. Karkamkar, Y. J. Choi, N. Tsumori, E. Rönnebro, T. Autrey, H. Shioyama, Q. Xu, *J. Am. Chem. Soc.* **2012**, *134*, 13926.
- [29] R. Q. Zou, H. Sakurai, S. Han, R. Q. Zhong, Q. Xu, *J. Am. Chem. Soc.* **2007**, *129*, 8402.
- [30] J. Y. Lee, O. K. Farha, J. Roberts, K. A. Scheidt, S. T. Nguyen, J. T. Hupp, *Chem. Soc. Rev.* **2009**, *38*, 1450, and references therein.
- [31] A. Corma, H. García, F. X. Llabrés-Xamena, *Chem. Rev.* **2010**, *110*, 4606.
- [32] J.-L. Wang, C. Wang, W. Lin, *ACS Catal.* **2012**, *2*, 2630.
- [33] Q.-L. Zhu, Q. Xu, *Chem* **2016**, *1*, 220.
- [34] X. Gu, Z.-H. Lu, H.-L. Jiang, T. Akita, Q. Xu, *J. Am. Chem. Soc.* **2011**, *133*, 11822.
- [35] P.-Z. Li, K. Aranishi, Q. Xu, *Chem. Commun.* **2012**, *48*, 3173.
- [36] Q.-L. Zhu, J. Li, Q. Xu, *J. Am. Chem. Soc.* **2013**, *135*, 10210.
- [37] P. Pachfule, X. Yang, Q.-L. Zhu, N. Tsumori, T. Uchida, Q. Xu, *J. Mater. Chem. A* **2017**, *5*, 4835.
- [38] F.-Y. Yi, D. Chen, M.-K. Wu, L. Han, H.-L. Jiang, *ChemPlusChem* **2016**, *81*, 675.
- [39] B. L. Chen, S. C. Xiang, G. D. Qian, *Acc. Chem. Res.* **2010**, *43*, 1115.
- [40] L. E. Kreno, K. Leong, O. K. Farha, M. Allendorf, R. P. V. Duyne, J. T. Hupp, *Chem. Rev.* **2012**, *112*, 1105, and references therein.
- [41] Z. Hu, B. J. Deibert, J. Li, *Chem. Soc. Rev.* **2014**, *43*, 5815.
- [42] P. Horcajada, R. Gref, T. Baati, P. K. Allan, G. Maurin, P. Couvreur, G. Férey, R. E. Morris, C. Serre, *Chem. Rev.* **2012**, *112*, 1232, and references therein.
- [43] C. He, D. Liu, W. Lin, *Chem. Rev.* **2015**, *115*, 11079.
- [44] Y. Cui, Y. Yue, G. Qian, B. Chen, *Chem. Rev.* **2012**, *112*, 1126.
- [45] P. Cheng, *Lanthanide Metal–Organic Frameworks, Structure and Bonding Series*, Springer, New York, USA **2015**.
- [46] Y. Bai, Y. Dou, L.-H. Xie, W. Rutledge, J.-R. Li, H.-C. Zhou, *Chem. Soc. Rev.* **2016**, *45*, 2327.
- [47] H.-L. Jiang, Q. Xu, *Chem. Commun.* **2011**, *47*, 3351.
- [48] H.-Q. Xu, J. Hu, D. Wang, Z. Li, Q. Zhang, Y. Luo, S.-H. Yu, H.-L. Jiang, *J. Am. Chem. Soc.* **2015**, *137*, 13440.
- [49] Q. Yang, Q. Xu, S.-H. Yu, H.-L. Jiang, *Angew. Chem.* **2016**, *128*, 3894; Q. Yang, Q. Xu, S.-H. Yu, H.-L. Jiang, *Angew. Chem., Int. Ed.* **2016**, *55*, 3685.
- [50] Y. V. Kaneti, J. Tang, R. R. Salunkhe, X. Jiang, A. Yu, K. C. W. Wu, Y. Yamauchi, *Adv. Mater.* **2017**, *29*, 1604898.
- [51] Y.-B. Huang, J. Liang, X.-S. Wang, R. Cao, *Chem. Soc. Rev.* **2017**, *46*, 126.
- [52] H. He, J. A. Perman, G. Zhu, S. Ma, *Small* **2016**, *12*, 6309.
- [53] M. Zhao, Q. Lu, Q. Ma, H. Zhang, *Small Methods* **2017**, *1*, 1600030.
- [54] M. D. Allendorf, C. A. Bauer, R. K. Bhakta, R. J. T. Houk, *Chem. Soc. Rev.* **2009**, *38*, 1330, and references therein.
- [55] K. Shen, X. Chen, J. Chen, Y. Li, *ACS Catal.* **2016**, *6*, 5887.
- [56] Q. G. Zhai, X. Bu, C. Mao, X. Zhao, L. Daemen, Y. Cheng, A. J. Ramirez-Cuesta, P. Feng, *Nat. Commun.* **2016**, *7*, 13645.
- [57] H. Wang, Q.-L. Zhu, R. Zou, Q. Xu, *Chem* **2017**, *2*, 52.
- [58] L. Wang, Y. Han, X. Feng, J. Zhou, P. Qi, B. Wang, *Coord. Chem. Rev.* **2016**, *307*, 361.
- [59] Q. Yang, Q. Xu, H.-L. Jiang, *Chem. Soc. Rev.* **2017**, *43*, 4774.
- [60] S.-L. Li, Q. Xu, *Energy Environ. Sci.* **2013**, *6*, 1656.
- [61] W. Xia, A. Mahmood, R. Zou, Q. Xu, *Energy Environ. Sci.* **2015**, *8*, 1837.
- [62] J.-K. Sun, Q. Xu, *Energy Environ. Sci.* **2014**, *7*, 2071.
- [63] X. Pei, Y. Chen, S. Li, S. Zhang, X. Feng, J. Zhou, B. Wang, *Chin. J. Chem.* **2016**, *34*, 157.
- [64] X.-W. Liu, T.-J. Sun, J.-L. Hu, S.-D. Wang, *J. Mater. Chem. A* **2016**, *4*, 3584.
- [65] F.-S. Ke, Y.-S. Wu, H. Deng, *J. Solid State Chem.* **2015**, *223*, 109.
- [66] F. Zheng, Y. Yang, Q. Chen, *Nat. Commun.* **2014**, *5*, 5261.
- [67] H.-L. Jiang, B. Liu, Y.-Q. Lan, K. Kuratani, T. Akita, H. Shioyama, F. Zong, Q. Xu, *J. Am. Chem. Soc.* **2011**, *133*, 11854.
- [68] Y. Guan, L. Yu, X. W. Lou, *Energy Environ. Sci.* **2016**, *9*, 3092.
- [69] Y.-Z. Chen, C. Wang, Z.-Y. Wu, Y. Xiong, Q. Xu, S.-H. Yu, H.-L. Jiang, *Adv. Mater.* **2015**, *27*, 5010.
- [70] Z. Li, M. Shao, L. Zhou, R. Zhang, C. Zhang, M. Wei, D. G. Evans, X. Duan, *Adv. Mater.* **2016**, *28*, 2337.
- [71] Q. Lin, X. Bu, A. Kong, C. Mao, X. Zhao, F. Bu, P. Feng, *J. Am. Chem. Soc.* **2015**, *137*, 2235.
- [72] L. Jiao, Y.-X. Zhou, H.-L. Jiang, *Chem. Sci.* **2016**, *7*, 1690.
- [73] S. Zhao, H. Yin, L. Du, L. He, K. Zhao, L. Chang, G. Yin, H. Zhao, S. Liu, Z. Tang, *ACS Nano* **2014**, *8*, 12660.
- [74] B. Liu, H. Shioyama, T. Akita, Q. Xu, *J. Am. Chem. Soc.* **2008**, *130*, 5390.
- [75] B. Liu, H. Shioyama, H.-L. Jiang, X. Zhang, Q. Xu, *Carbon* **2010**, *48*, 456.
- [76] P. Pachfule, D. Shinde, M. Majumder, Q. Xu, *Nat. Chem.* **2016**, *8*, 718.
- [77] A. Aijaz, N. Fujiwara, Q. Xu, *J. Am. Chem. Soc.* **2014**, *136*, 6790.
- [78] Q.-L. Zhu, W. Xia, T. Akita, R. Zou, Q. Xu, *Adv. Mater.* **2016**, *28*, 6391.
- [79] L.-F. Chen, Y. Lu, L. Yu, X. W. Lou, *Energy Environ. Sci.* **2017**, *10*, 1777.
- [80] W. Xia, C. Qu, Z. Liang, B. Zhao, S. Dai, B. Qiu, Y. Jiao, Q. Zhang, X. Huang, W. Guo, D. Dang, R. Zou, D. Xia, Q. Xu, M. Liu, *Nano Lett.* **2017**, *17*, 2788.
- [81] Q.-L. Zhu, W. Xia, L.-R. Zheng, R. Zou, Z. Liu, Q. Xu, *ACS Energy Lett.* **2017**, *2*, 504.
- [82] N. Stock, S. Biswas, *Chem. Rev.* **2012**, *112*, 933.
- [83] S. Qiu, G. Zhu, *Coord. Chem. Rev.* **2009**, *253*, 2891.
- [84] K. F. Babu, M. A. Kulandainathan, I. Katsounaros, L. Rassaei, A. D. Burrows, P. R. Raithby, F. Marken, *Electrochem. Commun.* **2010**, *12*, 632.
- [85] J. W. Shin, M. Kim, J. Cirera, S. Chen, G. J. Halder, T. A. Yersak, F. Paesani, S. M. Cohen, Y. S. Meng, *J. Mater. Chem. A* **2015**, *3*, 4738.
- [86] Q. Liu, L. Yu, Y. Wang, Y. Ji, J. Horvat, M.-L. Cheng, X. Jia, G. Wang, *Inorg. Chem.* **2013**, *52*, 2817.
- [87] M. Nagarathinam, K. Saravanan, E. J. H. Phua, M. V. Reddy, B. V. R. Chowdari, J. J. Vittal, *Angew. Chem.* **2012**, *124*, 5968; M. Nagarathinam, K. Saravanan, E. J. H. Phua, M. V. Reddy, B. V. R. Chowdari, J. J. Vittal, *Angew. Chem., Int. Ed.* **2012**, *51*, 5866.
- [88] S. Kim, K. W. Dawson, B. S. Gelfand, J. M. Taylor, G. K. H. Shimizu, *J. Am. Chem. Soc.* **2013**, *135*, 963.
- [89] J. Mao, L. Yang, P. Yu, X. Wei, L. Mao, *Electrochem. Commun.* **2012**, *19*, 29.
- [90] C. Zhang, M. Wang, L. Liu, X. Yang, X. Xu, *Electrochem. Commun.* **2013**, *33*, 131.

- [91] L. Yang, S. Kinoshita, T. Yamada, S. Kanda, H. Kitagawa, M. Tokunaga, T. Ishimoto, T. Ogura, R. Nagumo, A. Miyamoto, M. Koyama, *Angew. Chem.* **2010**, *122*, 5476; L. Yang, S. Kinoshita, T. Yamada, S. Kanda, H. Kitagawa, M. Tokunaga, T. Ishimoto, T. Ogura, R. Nagumo, A. Miyamoto, M. Koyama, *Angew. Chem., Int. Ed.* **2010**, *49*, 5348.
- [92] X.-F. Lu, P.-Q. Liao, J.-W. Wang, J.-X. Wu, X.-W. Chen, C.-T. He, J.-P. Zhang, G.-R. Li, X.-M. Chen, *J. Am. Chem. Soc.* **2016**, *138*, 8336.
- [93] H. Wang, F. Yin, G. Li, B. Chen, Z. Wang, *Int. J. Hydrogen Energy* **2014**, *39*, 16179.
- [94] J.-Q. Shen, P.-Q. Liao, D.-D. Zhou, C.-T. He, J.-X. Wu, W.-X. Zhang, J.-P. Zhang, X.-M. Chen, *J. Am. Chem. Soc.* **2017**, *139*, 1778.
- [95] S. Zhao, Y. Wang, J. Dong, C.-T. He, H. Yin, P. An, K. Zhao, X. Zhang, C. Gao, L. Zhang, J. Lv, J. Wang, J. Zhang, A. M. Khattak, N. A. Khan, Z. Wei, J. Zhang, S. Liu, H. Zhao, Z. Tang, *Nat. Energy* **2016**, *1*, 16184.
- [96] L. M. Rodriguez-Albelo, A. R. Ruiz-Salvador, A. Sampieri, D. W. Lewis, A. Gómez, B. Nohra, P. Mialane, J. Marrot, F. Sécheresse, C. Mellot-Draznieks, R. N. Biboum, B. Keita, L. Nadjó, A. Dolbecq, *J. Am. Chem. Soc.* **2009**, *131*, 16078.
- [97] B. Nohra, H. E. Moll, L. M. R. Albelo, P. Mialane, J. Marrot, C. Mellot-Draznieks, M. O'Keeffe, R. N. Biboum, J. Lemaire, B. Keita, L. Nadjó, A. Dolbecq, *J. Am. Chem. Soc.* **2011**, *133*, 13363.
- [98] J.-S. Qin, D.-Y. Du, W. Guan, X.-J. Bo, Y.-F. Li, L.-P. Guo, Z.-M. Su, Y.-Y. Wang, Y.-Q. Lan, H.-C. Zhou, *J. Am. Chem. Soc.* **2015**, *137*, 7169.
- [99] I. M. Mbomekalle, B. Keita, L. Nadjó, P. Berthet, K. I. Hardcastle, C. L. Hill, T. M. Anderson, *Inorg. Chem.* **2003**, *42*, 1163.
- [100] Y. Gong, T. Wu, P. G. Jiang, J. H. Lin, Y. X. Yang, *Inorg. Chem.* **2013**, *52*, 777.
- [101] Y. Gong, J. Li, P.-G. Jiang, Q.-F. Li, J.-H. Lin, *Dalton Trans.* **2013**, *42*, 1603.
- [102] Z. Zhang, H. Yoshikawa, K. Awaga, *J. Am. Chem. Soc.* **2014**, *136*, 16112.
- [103] D. Sheberla, J. C. Bachman, J. S. Elias, C.-J. Sun, Y. Shao-Horn, M. Dinc, *Nat. Mater.* **2017**, *16*, 220.
- [104] Y. Lin, Q. Zhang, C. Zhao, H. Li, C. Kong, C. Shen, L. Chen, *Chem. Commun.* **2015**, *51*, 697.
- [105] Y. Tan, W. Zhang, Y. Gao, J. Wu, B. Tang, *RSC Adv.* **2015**, *5*, 17601.
- [106] D. Wu, Z. Guo, X. Yin, Q. Pang, B. Tu, L. Zhang, Y.-G. Wang, Q. Li, *Adv. Mater.* **2014**, *26*, 3258.
- [107] D. Y. Lee, S. J. Yoon, N. K. Shrestha, S.-H. Lee, H. Ahn, S.-H. Han, *Microporous Mesoporous Mater.* **2012**, *153*, 163.
- [108] A. Shigematsu, T. Yamada, H. Kitagawa, *J. Am. Chem. Soc.* **2011**, *133*, 2034.
- [109] S. Horike, D. Umeyama, S. Kitagawa, *Acc. Chem. Res.* **2013**, *46*, 2376.
- [110] I. Hod, W. Bury, D. M. Karlin, P. Deria, C.-W. Kung, M. J. Katz, M. So, B. Klahr, D. Jin, Y.-W. Chung, T. W. Odom, O. K. Farha, J. T. Hupp, *Adv. Mater.* **2014**, *26*, 6295.
- [111] Y. Xu, X.-B. Yin, X.-W. He, Y.-K. Zhang, *Biosens. Bioelectron.* **2015**, *68*, 197.
- [112] X. Fu, D. Yu, J. Zhou, S. Li, X. Gao, Y. Han, P. Qi, X. Feng, B. Wang, *CrystEngComm* **2016**, *18*, 4236.
- [113] T. Yamada, M. Sadakiyo, H. Kitagawa, *J. Am. Chem. Soc.* **2009**, *131*, 3144.
- [114] M. G. Goesten, J. Juan-Alcañiz, E. V. Ramos-Fernandez, K. B. S. S. Gupta, E. Stavitski, H. V. Bekkum, J. Gascon, F. Kapteijn, *J. Catal.* **2011**, *281*, 177.
- [115] E. Pardo, C. Train, G. Gontard, K. Boubekeur, O. Fabelo, H. Liu, B. Dkhil, F. Lloret, K. Nakagawa, H. Tokoro, S.-i. Ohkoshi, M. Verdaguier, *J. Am. Chem. Soc.* **2011**, *133*, 15328.
- [116] S. C. Sahoo, T. Kundu, R. Banerjee, *J. Am. Chem. Soc.* **2011**, *133*, 17950.
- [117] N. C. Jeong, B. Samanta, C. Y. Lee, O. K. Farha, J. T. Hupp, *J. Am. Chem. Soc.* **2012**, *134*, 51.
- [118] M. Sadakiyo, H. O kawa, A. Shigematsu, M. Ohba, T. Yamada, H. Kitagawa, *J. Am. Chem. Soc.* **2012**, *134*, 5472.
- [119] R. Ameloot, M. Aubrey, B. M. Wiers, A. P. Gómora-Figueroa, S. N. Patel, N. P. Balsara, J. R. Long, *Chem. – Eur. J.* **2013**, *19*, 5533.
- [120] G. Xu, K. Otsubo, T. Yamada, S. Sakaida, H. Kitagawa, *J. Am. Chem. Soc.* **2013**, *135*, 7438.
- [121] A. A. Talin, A. Centrone, A. C. Ford, M. E. Foster, V. Stavila, P. Haney, R. A. Kinney, V. Szalai, F. E. Gabaly, H. P. Yoon, F. Léonard, M. D. Allendorf, *Science* **2014**, *343*, 66.
- [122] J. M. Taylor, R. K. Mah, I. L. Moudrakovski, C. I. Ratcliffe, R. Vaidhyanathan, G. K. H. Shimizu, *J. Am. Chem. Soc.* **2010**, *132*, 14055.
- [123] D. Umeyama, S. Horike, M. Inukai, T. Itakura, S. Kitagawa, *J. Am. Chem. Soc.* **2012**, *134*, 12780.
- [124] V. G. Ponomareva, K. A. Kovalenko, A. P. Chupakhin, D. N. Dybtsev, E. S. Shutova, V. P. Fedin, *J. Am. Chem. Soc.* **2012**, *134*, 15640.
- [125] J. A. Hurd, R. Vaidhyanathan, V. Thangadurai, C. I. Ratcliffe, I. L. Moudrakovski, G. K. H. Shimizu, *Nat. Chem.* **2009**, *1*, 705.
- [126] S. S. Nagarkar, S. M. Unni, A. Sharma, S. Kurungot, S. K. Ghosh, *Angew. Chem.* **2014**, *126*, 2676; S. S. Nagarkar, S. M. Unni, A. Sharma, S. Kurungot, S. K. Ghosh, *Angew. Chem., Int. Ed.* **2014**, *53*, 2638.
- [127] C. Li, X. Lou, M. Shen, X. Hu, Z. Guo, Y. Wang, B. Hu, Q. Chen, *ACS Appl. Mater. Interfaces* **2016**, *8*, 15352.
- [128] C. Combelles, M. Ben Yahia, L. Pedesseau, M.-L. Doublet, *J. Phys. Chem. C* **2010**, *114*, 9518.
- [129] D. Y. Lee, D. V. Shinde, E.-K. Kim, W. Lee, I.-W. Oh, N. K. Shrestha, J. K. Lee, S.-H. Han, *Microporous Mesoporous Mater.* **2013**, *171*, 53.
- [130] C. Liao, Y. Zuo, W. Zhang, J. Zhao, B. Tang, A. Tang, Y. Sun, J. Xu, *Russ. J. Electrochem.* **2013**, *49*, 983.
- [131] K. M. Choi, H. M. Jeong, J. H. Park, Y.-B. Zhang, J. K. Kang, O. M. Yaghi, *ACS Nano* **2014**, *8*, 7451.
- [132] J. Yang, P. Xiong, C. Zheng, H. Qiu, M. Wei, *J. Mater. Chem. A* **2014**, *2*, 16640.
- [133] L. Kang, S.-X. Sun, L.-B. Kong, J.-W. Lang, Y.-C. Luo, *Chin. Chem. Lett.* **2014**, *25*, 957.
- [134] L. Sun, M. G. Campbell, M. Dinc, *Angew. Chem.* **2016**, *128*, 3628; L. Sun, M. G. Campbell, M. Dinc, *Angew. Chem., Int. Ed.* **2016**, *55*, 3566.
- [135] G. D. Combarieu, M. Morcrette, F. Millange, N. Guillou, J. Cabana, C. P. Grey, I. Margiolaki, G. Férey, J.-M. Tarascon, *Chem. Mater.* **2009**, *21*, 1602.
- [136] Q.-L. Zhu, Q. Xu, *Chem. Soc. Rev.* **2014**, *43*, 5468, and references therein.
- [137] S. Li, F. Huo, *Nanoscale* **2015**, *7*, 7482, and references therein.
- [138] X. Li, F. Cheng, S. Zhang, J. Chen, *J. Power Sources* **2006**, *160*, 542.
- [139] C. Combelles, M.-L. Doublet, *Ionics* **2008**, *14*, 279.
- [140] G. D. Combarieu, S. Hamelet, F. Millange, M. Morcrette, J.-M. Tarascon, G. Férey, R. I. Walton, *Electrochem. Commun.* **2009**, *11*, 1881.
- [141] K. Saravanan, M. Nagarathinam, P. Balaya, J. J. Vittal, *J. Mater. Chem.* **2010**, *20*, 8329.
- [142] B. M. Wiers, M.-L. Foo, N. P. Balsara, J. R. Long, *J. Am. Chem. Soc.* **2011**, *133*, 14522.
- [143] R. Demir-Cakan, M. Morcrette, F. Nouar, C. Davoisne, T. Devic, D. Gonbeau, R. Dominko, C. Serre, G. Férey, J.-M. Tarascon, *J. Am. Chem. Soc.* **2011**, *133*, 16154.
- [144] Z. Wang, X. Li, Y. Cui, Y. Yang, H. Pan, Z. Wang, C. Wu, B. Chen, G. Qian, *Cryst. Growth Des.* **2013**, *13*, 5116.

- [145] R. Chen, T. Zhao, T. Tian, S. Cao, P. R. Coxon, K. Xi, D. Fairen-Jimenez, R. Vasant Kumar, A. K. Cheetham, *APL Mater.* **2014**, *2*, 124109.
- [146] J. Zhou, R. Li, X. Fan, Y. Chen, R. Han, W. Li, J. Zheng, B. Wang, X. Li, *Energy Environ. Sci.* **2014**, *7*, 2715.
- [147] J. Zhou, X. Yu, X. Fan, X. Wang, H. Li, Y. Zhang, W. Li, J. Zheng, B. Wang, X. Li, *J. Mater. Chem. A* **2015**, *3*, 8272.
- [148] Z. Wang, Z. Dou, Y. Cui, Y. Yang, Z. Wang, G. Qian, *Microporous Mesoporous Mater.* **2014**, *185*, 92.
- [149] T. An, Y. Wang, J. Tang, Y. Wang, L. Zhang, G. Zheng, *J. Colloid Interface Sci.* **2015**, *445*, 320.
- [150] W. Kaveevivitchai, A. J. Jacobson, *J. Power Sources* **2015**, *278*, 265.
- [151] J. Zheng, J. Tian, D. Wu, M. Gu, W. Xu, C. Wang, F. Gao, M. H. Engelhard, J.-G. Zhang, J. Liu, J. Xiao, *Nano Lett.* **2014**, *14*, 2345.
- [152] M. Meilikhov, K. Yusenko, D. Esken, S. Turner, G. V. Tendeloo, R. A. Fischer, *Eur. J. Inorg. Chem.* **2010**, *2010*, 3701.
- [153] R. Díaz, M. G. Orcajo, J. A. Botas, G. Calleja, J. Palma, *Mater. Lett.* **2012**, *68*, 126.
- [154] D. K. Yadava, V. Ganesana, F. Markenb, R. Guptaa, P. K. Sonkara, *Electrochim. Acta* **2016**, *219*, 482.
- [155] J. Yang, C. Zheng, P. Xiong, Y. Lia, M. Wei, *J. Mater. Chem. A* **2014**, *2*, 19005.
- [156] C. T. Pereira de Silva, F. R. Veregue, L. W. Aguiar, J. G. Meneguim, M. P. Moisés, S. L. Fávaro, E. Radovanovic, E. M. Girotoia, A. W. Rinaldi, *New J. Chem.* **2016**, *40*, 8872.
- [157] D. K. Yadav, V. Ganesan, P. K. Sonkar, R. Gupta, P. K. Rastogi, *Electrochim. Acta* **2016**, *200*, 276.
- [158] P. Miao, G. Li, G. Zhang, H. Lu, *J. Energy Chem.* **2014**, *23*, 507.
- [159] H. Wang, F. Yin, B. Chen, G. Li, *J. Mater. Chem. A* **2015**, *3*, 16168.
- [160] Y. Gao, J. Wu, W. Zhang, Y. Tan, J. Zhao, B. Tang, *Mater. Lett.* **2014**, *128*, 208.
- [161] J. Yang, H. Ye, F. Zhao, B. Zeng, *ACS Appl. Mater. Interfaces* **2016**, *8*, 20407.
- [162] W.-W. Zhan, Q. Kuang, J.-Z. Zhou, X.-J. Kong, Z.-X. Xie, L.-S. Zheng, *J. Am. Chem. Soc.* **2013**, *135*, 1926.
- [163] Y. Gao, J. Wu, W. Zhang, Y. Tan, J. Gao, B. Tang, J. Zhao, *RSC Adv.* **2014**, *4*, 36366.
- [164] L. Hu, N. Wu, J. Zheng, J.-L. Xu, M. Zhang, P.-G. He, *Anal. Sci.* **2014**, *30*, 663.
- [165] Z. Li, Y. Tan, W. Zhang, B. Tang, *Ionics* **2016**, *22*, 2545.
- [166] Y. Han, P. Qi, X. Feng, S. Li, X. Fu, H. Li, Y. Chen, J. Zhou, X. Li, B. Wang, *ACS Appl. Mater. Interfaces* **2015**, *7*, 2178.
- [167] D. Kim, D. R. Whang, S. Y. Park, *J. Am. Chem. Soc.* **2016**, *138*, 8698.
- [168] X. Dai, M. Liu, Z. Li, A. Jin, Y. Ma, X. Huang, H. Sun, H. Wang, X. Zhang, *J. Phys. Chem. C* **2016**, *120*, 12539.
- [169] S. Dong, D. Zhang, G. Suo, W. Wei, T. Huang, *Anal. Chim. Acta* **2016**, *934*, 203.
- [170] Y.-Z. Zhang, T. Cheng, Y. Wang, W.-Y. Lai, H. Pang, W. Huang, *Adv. Mater.* **2016**, *28*, 5242.
- [171] G. Jia, W. Zhang, Z. Jin, W. An, Y. Gao, X. Zhang, J. Liu, *Electrochim. Acta* **2014**, *144*, 1.
- [172] P. Srimuk, S. Luanwuthi, A. Krittayavathananon, M. Sawangphruk, *Electrochim. Acta* **2015**, *157*, 69.
- [173] M. Saraf, R. Rajakb, S. M. Mobin, *J. Mater. Chem. A* **2016**, *4*, 16432.
- [174] M. Jahan, Z. Liu, K. P. Loh, *Adv. Funct. Mater.* **2013**, *23*, 5363.
- [175] W. Zhang, Y. Tan, Y. Gao, J. Wu, J. Hu, A. Stein, B. Tang, *J. Appl. Electrochem.* **2016**, *46*, 441.
- [176] M. Jahan, Q. Bao, K. P. Loh, *J. Am. Chem. Soc.* **2012**, *134*, 6707.
- [177] Z. Zhao, S. Wang, R. Liang, Z. Li, Z. Shi, G. Chen, *J. Mater. Chem. A* **2014**, *2*, 13509.
- [178] W. Bao, Z. Zhang, Y. Qua, C. Zhou, X. Wang, J. Li, *J. Alloys Compd.* **2014**, *582*, 334.
- [179] Y. Zhang, B. Lin, Y. Sun, X. Zhang, H. Yang, J. Wang, *RSC Adv.* **2015**, *5*, 58100.
- [180] J. Zhou, X. Li, L. Yang, S. Yan, M. Wang, D. Cheng, Q. Chen, Y. Dong, P. Liu, W. Cai, C. Zhang, *Anal. Chim. Acta* **2015**, *899*, 57.
- [181] E. Zhou, Y. Zhang, Y. Li, X. He, *Electroanalysis* **2014**, *26*, 2526.
- [182] Y. Song, C. Gong, D. Su, Y. Shen, Y. Song, L. Wang, *Anal. Methods* **2016**, *8*, 2290.
- [183] Y. Zhang, X. Bo, A. Nsabimana, C. Han, M. Li, L. Guo, *J. Mater. Chem. A* **2015**, *3*, 732.
- [184] Y. Mao, J. Li, W. Cao, Y. Ying, P. Hu, Y. Liu, L. Sun, H. Wang, C. Jin, X. Peng, *Nat. Commun.* **2014**, *5*, 5532.
- [185] P. C. Banerjee, D. E. Lobo, R. Middag, W. K. Ng, M. E. Shaibani, M. Majumder, *ACS Appl. Mater. Interfaces* **2015**, *7*, 3655.
- [186] Y. Jin, C. Zhao, Z. Sun, Y. Lin, L. Chen, D. Wang, C. Shen, *RSC Adv.* **2016**, *6*, 30763.
- [187] L. Wang, H. Yang, J. He, Y. Zhang, J. Yu, Y. Song, *Electrochim. Acta* **2016**, *213*, 691.
- [188] D. Fu, H. Li, X.-M. Zhang, G. Han, H. Zhou, Y. Chang, *Mater. Chem. Phys.* **2016**, *179*, 166.
- [189] Y. Yue, B. Guo, Z.-A. Qiao, P. F. Fulvio, J. Chen, A. J. Binder, C. Tian, S. Dai, *Microporous Mesoporous Mater.* **2014**, *198*, 139.
- [190] M. Jiang, L. Li, D. Zhu, H. Zhang, X. Zhao, *J. Mater. Chem. A* **2014**, *2*, 5323.
- [191] J. Yang, F. Zhao, B. Zeng, *RSC Adv.* **2015**, *5*, 22060.
- [192] B. Yuan, J. Zhang, R. Zhang, H. Shi, X. Guo, Y. Guo, X. Guo, S. Cai, D. Zhang, *Int. J. Electrochem. Sci.* **2015**, *10*, 4899.
- [193] P. Wen, P. Gong, J. Sun, J. Wang, S. Yang, *J. Mater. Chem. A* **2015**, *3*, 13874.
- [194] X. Kang, Q. Zhu, X. Sun, J. Hu, J. Zhang, Z. Liu, B. Han, *Chem. Sci.* **2016**, *7*, 266.
- [195] Y. Fang, X. Li, F. Li, X. Lin, M. Tian, X. Long, X. An, Y. Fu, J. Jin, J. Ma, *J. Power Sources* **2016**, *326*, 50.
- [196] Z. Ghiamaty, A. Ghaffarinejad, M. Faryadras, A. Abdolmaleki, H. Kazemi, *J. Nanostruct. Chem.* **2016**, *6*, 299.
- [197] Y. Yan, P. Gu, S. Zheng, M. Zheng, H. Pang, H. Xue, *J. Mater. Chem. A* **2016**, *4*, 19078.
- [198] X. Wang, H. Zhao, H. Lin, G. Liu, J. Fang, B. Chen, *Electroanalysis* **2008**, *20*, 1055.
- [199] H. Y. Lin, X. Wang, H. Hu, B. Chen, G. Liu, *Solid State Sci.* **2009**, *11*, 643.
- [200] C. Hou, J. Peng, Q. Xu, Z. Jia, X. Hu, *RSC Adv.* **2012**, *2*, 12696.
- [201] C. Yuan, J. Li, P. Han, Y. Lai, Z. Zhang, J. Liu, *J. Power Sources* **2013**, *240*, 653.
- [202] C. Gerbaldi, J. R. Nair, M. A. Kulandainathan, S. Kumar, C. Ferrara, P. Mustarell, A. M. Stephan, *J. Mater. Chem. A* **2014**, *2*, 9948.
- [203] N. Angulakshmi, R. S. Kumar, M. A. Kulandainathan, A. M. Stephan, *J. Phys. Chem. C* **2014**, *118*, 24240.
- [204] R. S. Kumar, M. Raja, M. A. Kulandainathana, A. M. Stephan, *RSC Adv.* **2014**, *4*, 26171.
- [205] K. Zhu, Y. Liu, J. Liu, *RSC Adv.* **2014**, *4*, 42278.
- [206] I. Hod, P. Deria, W. Bury, J. E. Mondloch, C.-W. Kung, M. So, M. D. Sampson, A. W. Peters, C. P. Kubiak, O. K. Farha, J. T. Hupp, *Nat. Commun.* **2015**, *6*, 8304.
- [207] L. Yang, C. Xu, W. Ye, W. Liu, *Sens. Actuators, B* **2015**, *215*, 489.
- [208] S. D. Worrall, H. Mann, A. Rogers, M. A. Bissett, M. P. Attfield, R. A. W. Dryfe, *Electrochim. Acta* **2016**, *197*, 228.
- [209] B. Yuan, J. Zhang, R. Zhang, H. Shi, N. Wang, J. Li, F. Ma, D. Zhang, *Sens. Actuators, B* **2016**, *222*, 632.
- [210] S. D. Worrall, M. A. Bissett, W. Hirunpinyopas, M. P. Attfield, R. A. W. Dryfe, *J. Mater. Chem. C* **2016**, *4*, 8687.
- [211] M. Naseri, L. Fotouhi, A. Ehsani, S. Dehghanpour, *J. Colloid Interface Sci.* **2016**, *484*, 314.
- [212] E. Shi, X. Zou, J. Liu, H. Lin, F. Zhang, S. Shi, F. Liu, G. Zhu, F. Qu, *Dalton Trans.* **2016**, *45*, 7728.



- [213] C.-W. Kung, Y.-S. Li, M.-H. Lee, S.-Y. Wang, W.-H. Chiang, K.-C. Ho, *J. Mater. Chem. A* **2016**, *4*, 10673.
- [214] L. Cronin, P. A. McGregor, S. Parsons, S. Teat, R. O. Gould, V. A. White, N. J. Long, N. Robertson, *Inorg. Chem.* **2004**, *43*, 8023.
- [215] E. A. Medlycott, G. S. Hanan, *Chem. Commun.* **2007**, 4884.
- [216] C. Streb, C. Ritchie, D.-L. Long, P. Kögerler, L. Cronin, *Angew. Chem.* **2007**, *119*, 7723; C. Streb, C. Ritchie, D.-L. Long, P. Kögerler, L. Cronin, *Angew. Chem., Int. Ed.* **2007**, *46*, 7579.
- [217] S.-T. Zheng, J. Zhang, G.-Y. Yang, *Angew. Chem.* **2008**, *120*, 3973; S.-T. Zheng, J. Zhang, G.-Y. Yang, *Angew. Chem., Int. Ed.* **2008**, *47*, 3909.
- [218] J. M. Clemente-Juan, E. Coronado, *Coord. Chem. Rev.* **1999**, *193–195*, 361.
- [219] C. L. Hill, *J. Mol. Catal. A: Chem* **2007**, *262*, 2.
- [220] H. N. Miras, J. Yan, D.-L. Long, L. Cronin, *Chem. Soc. Rev.* **2012**, *41*, 7403.
- [221] D.-Y. Du, L.-K. Yan, Z.-M. Su, S.-L. Li, Y.-Q. Lan, E.-B. Wang, *Coord. Chem. Rev.* **2013**, *257*, 702.
- [222] H. N. Miras, L. Vilà-Nadal, L. Cronin, *Chem. Soc. Rev.* **2014**, *43*, 5679.
- [223] D.-Y. Du, J.-S. Qin, S.-L. Li, Z.-M. Su, Y.-Q. Lan, *Chem. Soc. Rev.* **2014**, *43*, 4615.
- [224] F. Vermoortele, R. Ameloot, A. Vimont, C. Serre, D. Vos, *Chem. Commun.* **2011**, *47*, 1521.
- [225] R. Vaidhyanathan, S. S. Iremonger, K. W. Dawson, G. K. H. Shimizu, *Chem. Commun.* **2009**, 5230.
- [226] F. S. Ke, B. C. Solomon, S. G. Ma, X. D. Zhou, *Electrochim. Acta* **2012**, *85*, 444.
- [227] X. Ji, K. T. Lee, L. F. Nazar, *Nat. Mater.* **2009**, *8*, 500.
- [228] N. A. Alhebshi, R. B. Rakhi, H. N. Alshareef, *J. Mater. Chem. A* **2013**, *1*, 14897.
- [229] H. Wang, Y. Liang, T. Mirfakhrai, Z. Chen, H. S. Casalongue, H. Dai, *Nano Res.* **2011**, *4*, 729.
- [230] H. Wang, H. S. Casalongue, Y. Liang, H. Dai, *J. Am. Chem. Soc.* **2010**, *132*, 7472.
- [231] M.-S. Wu, K.-C. Huang, *Int. J. Hydrogen Energy* **2011**, *36*, 13407.
- [232] L.-X. Yang, Y.-J. Zhu, H. Tong, Z.-H. Liang, W.-W. Wang, *Cryst. Growth Des.* **2007**, *7*, 2716.
- [233] H. Zhang, Y. Li, Y. Wang, J. Li, *ACS Nano* **2009**, *4*, 380.
- [234] A. Benvidi, M. D. Tezerjani, S. Jahanbani, M. M. Ardakani, S. M. Moshtaghioun, *Talanta* **2016**, *147*, 621.
- [235] Z. Q. Niu, J. Chen, H. H. Hng, J. Ma, X. D. Chen, *Adv. Mater.* **2012**, *24*, 4144.
- [236] S. Chen, W. Ma, Y. Cheng, Z. Weng, B. Sun, L. Wang, W. Chen, F. Li, M. Zhu, H.-M. Cheng, *Nano Energy* **2015**, *15*, 642.
- [237] J. X. Zhu, T. Zhu, X. Z. Zhou, Y. Y. Zhang, X. W. Lou, X. D. Chen, H. Zhang, H. H. Hng, Q. Y. Yan, *Nanoscale* **2011**, *3*, 1084.
- [238] Z. Wang, Y. Zhang, S. Liu, T. Zhang, *Sens. Actuators, B* **2016**, *222*, 893.
- [239] T. Ando, *NPG Asia Mater.* **2009**, *1*, 17.
- [240] S. Y. Yin, Y. Y. Zhang, J. H. Kong, C. J. Zou, C. M. Li, X. H. Lu, J. Ma, F. Y. C. Boey, X. D. Chen, *ACS Nano* **2011**, *5*, 3831.
- [241] A. M. Stephan, *Eur. Polym. J.* **2006**, *42*, 21.
- [242] A. M. Stephan, K. S. Nahm, *Polymer* **2006**, *47*, 5952.
- [243] C. A. Vincent, B. Scrosati, *Bull. Mater. Res. Soc.* **2000**, *25*, 28.
- [244] W.-J. Li, M. Tu, R. Cao, R. A. Fischer, *J. Mater. Chem. A* **2016**, *4*, 12356.
- [245] R. Ameloot, L. Stappers, J. Fransaer, L. Alaerts, B. F. Sels, D. E. De Vos, *Chem. Mater.* **2009**, *21*, 2580.
- [246] L. Wang, X. Feng, L. Ren, Q. Piao, J. Zhong, Y. Wang, H. Li, Y. Chen, B. Wang, *J. Am. Chem. Soc.* **2015**, *137*, 4920.
- [247] Q. Wang, D. O'Hare, *Chem. Rev.* **2012**, *112*, 4124, and references therein.
- [248] X. Guo, F. Zhang, D. G. Evans, X. Duan, *Chem. Commun.* **2010**, *46*, 5197, and references therein.
- [249] C. Li, M. Wei, D. G. Evans, X. Duan, *Small* **2014**, *10*, 4469, and references therein.
- [250] Y. Dou, J. Zhou, F. Yang, M.-J. Zhao, Z. Nie, J.-R. Li, *J. Mater. Chem. A* **2016**, *4*, 12526.